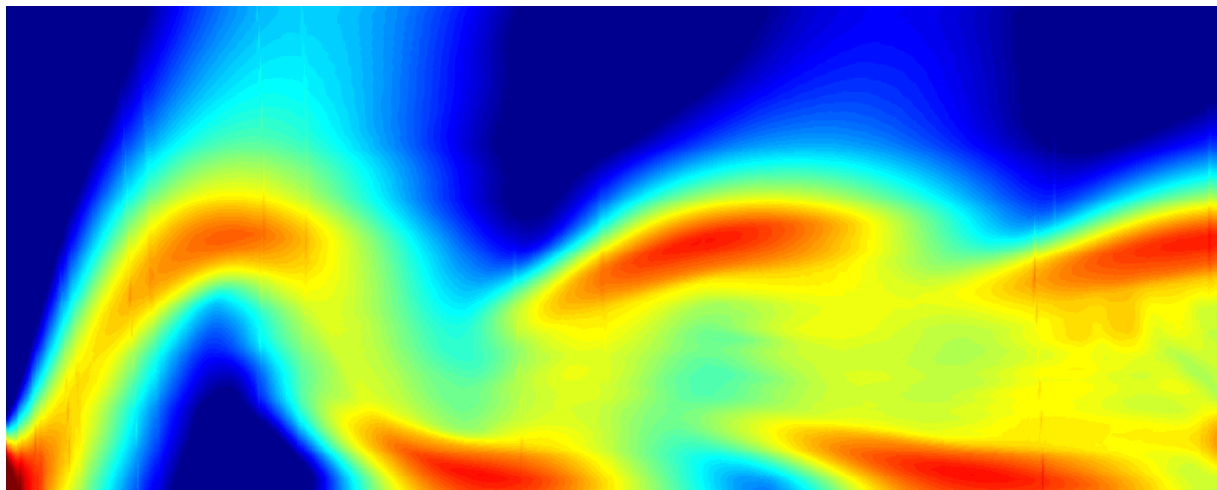


# CHALMERS



## Nonlinear outdoor sound propagation

A numerical implementation and study using the nonlinear progressive wave equation

Master's Thesis in the Master's programme in Sound and Vibration

**THOMAS LEISSING**

Department of Civil and Environmental Engineering

*Division of Division of Applied Acoustics*

*Vibroacoustics Group*

CHALMERS UNIVERSITY OF TECHNOLOGY

Göteborg, Sweden 2006

Master's Thesis 2007:13

MASTER'S THESIS 2007:13

Nonlinear outdoor sound propagation  
A numerical implementation and study using  
the nonlinear progressive wave equation

Master's Thesis in the Master's programme in Sound and  
Vibration

THOMAS LEISSING

Department of Civil and Environmental Engineering  
*Division of Applied Acoustics*  
*Vibroacoustics Group*  
CHALMERS UNIVERSITY OF TECHNOLOGY  
Göteborg, Sweden 2007

Nonlinear outdoor sound propagation  
A numerical implementation and study using the nonlinear progressive wave equation

© THOMAS LEISSING, 2007

Master's Thesis 2007:13

Department of Civil and Environmental Engineering  
Division of Applied Acoustics  
Vibroacoustics Group  
Chalmers University of Technology  
SE-41296 Göteborg  
Sweden

Tel. +46-(0)31 772 1000

**Cover:**

Transmission loss vertical map. A monopole source is placed on the ground; the sound celerity profile is complex. This configuration results in upward/downward propagation with several reflections on the ground.

Reproservice / Department of Civil and Environmental Engineering  
Göteborg, Sweden 2007

Nonlinear outdoor sound propagation

A numerical implementation and study using the nonlinear progressive wave equation

Master's Thesis in the Master's programme in Sound and Vibration

THOMAS LEISSING

Department of Civil and Environmental Engineering

Division of Applied Acoustics

Vibroacoustics Group

Chalmers University of Technology

## Abstract

This master's thesis carried out at the CSTB establishment in Grenoble (France) focuses on nonlinear effects in sound propagation. This restricts the kind of signals considered to high amplitude waves, usually higher than 100 Pa (134 dB re 20  $\mu$ Pa). Such acoustic pressures can come from sonic boom, gunshots or explosion waves. Nonlinearities in sound propagation will be responsible for wave signature modifications and the need to know exactly in which way the signal will change can be crucial in some applications, for example in the frame of military surveillance, or to study buildings response to blast wave. A time-domain numerical method that allows to simulate nonlinear propagation in a realistic environment is described and the validation of results is presented. The model established is then used to study the propagation of a blast wave. This case study is inspired from the explosion of a chemical warehouse that happened in the city of Toulouse (south-west of France) in September 2001. The last part of this master's thesis states a methodology that allows to couple different numerical models. This can be interesting for instance for using boundary element methods to study protection screen efficiency.

**Keywords:** nonlinear acoustics, outdoor sound propagation, long-range sound propagation, finite differences, explosion, blast wave, shock, N-wave.



# Contents

<b>Abstract</b>	<b>iii</b>
<b>Contents</b>	<b>iii</b>
<b>Acknowledgements</b>	<b>vii</b>
<b>1. Introduction</b>	<b>1</b>
1.1. CSTB . . . . .	1
1.2. Goals . . . . .	3
1.3. Content . . . . .	3
<b>2. Nonlinear outdoor sound propagation</b>	<b>5</b>
2.1. Geometrical spreading . . . . .	5
2.2. Atmospheric absorption . . . . .	5
2.3. Features due to the ground . . . . .	6
2.3.1. Path-length differences (PLD) . . . . .	7
2.3.2. Ground impedance . . . . .	7
2.4. Meteorological effects . . . . .	9
2.4.1. Relevant meteorological phenomena . . . . .	9
2.4.2. Refraction . . . . .	11
2.5. Nonlinear acoustics . . . . .	13
2.5.1. Wave equations of nonlinear acoustics . . . . .	14
<b>3. Computational method</b>	<b>17</b>
3.1. State of the art . . . . .	17
3.1.1. General time domain algorithm . . . . .	18
3.1.2. Time domain algorithm based on the NPE . . . . .	19
3.2. The nonlinear progressive wave equation . . . . .	20
3.2.1. Derivation and original formulation . . . . .	21
3.2.2. Cylindrical coordinates formulation . . . . .	24
3.2.3. High-angle formulation . . . . .	25
3.2.4. Thermoviscous effects . . . . .	25
3.3. Implementation of the NPE . . . . .	26

3.3.1.	Operator splitting . . . . .	26
3.3.2.	Nonlinear effects and refraction . . . . .	27
3.3.3.	Cylindrical decay . . . . .	28
3.3.4.	Thermoviscous effects . . . . .	30
3.3.5.	Diffraction . . . . .	31
3.3.6.	Boundary conditions . . . . .	32
3.4.	Numerical considerations . . . . .	35
<b>4.</b>	<b>Model validation</b>	<b>37</b>
4.1.	Nonlinear effects . . . . .	37
4.1.1.	Fubini's solution . . . . .	37
4.1.2.	Results . . . . .	37
4.2.	Complex linear case . . . . .	38
4.2.1.	ATMOS sound propagation code . . . . .	38
4.2.2.	Coupling with ATMOS . . . . .	40
4.2.3.	Results . . . . .	42
4.3.	Conclusion . . . . .	43
<b>5.</b>	<b>Case study</b>	<b>47</b>
5.1.	Configuration . . . . .	47
5.2.	Results . . . . .	48
5.3.	Coupling . . . . .	51
5.4.	Prediction model . . . . .	54
5.4.1.	Derivation . . . . .	54
5.4.2.	Results . . . . .	56
<b>6.</b>	<b>Conclusion and perspectives</b>	<b>59</b>
6.1.	Conclusion . . . . .	59
6.2.	Perspectives . . . . .	59
	<b>Bibliography</b>	<b>61</b>
	<b>Appendix</b>	<b>65</b>
	<b>A. Crank-Nicolson scheme and Thomas algorithm</b>	<b>67</b>
	<b>B. User interface to the NPE propagation code</b>	<b>69</b>

# Acknowledgements

I would like to first thank my advisors, Jérôme Defrance and Philippe Jean, for supporting me and giving me considerable freedom to determine the direction of this research. I would also like to thank François Abbaléa, who wrote the ATMOS code and helped me using it, and Frédéric Conte, whose work inspired this master's thesis. Finally, thanks to all the people with who I shared these six months and who made this period extremely pleasant.



# 1. Introduction

Environmental noise, including sounds from road/rail/air traffic, industries, construction, public work, and the neighbourhood, is often the main cause of environmental distress in terms of the number of complaints received. Research has been carried out in the area of environmental acoustics, including noise propagation prediction, noise control techniques, as well as psychological, physiological, social and economic effects of community noise.

This master's thesis carried out at the CSTB establishment in Grenoble (France) focuses on nonlinear effects in sound propagation. This restricts the kind of signals considered to high amplitude waves, usually higher than 100 Pa (134 dB re 20  $\mu$ Pa). Such acoustic pressures can come from sonic boom, gunshots or explosion waves. Nonlinearities in sound propagation will be responsible for wave signature modifications and the need to know exactly in which way the signal will change can be crucial in some applications, for example in the frame of military surveillance, or to study buildings response to blast wave. Nonlinear acoustics is a young discipline which interest arose with the apparition of high amplitude waves generators (jet noise, explosions). As a result different models, theoretical and numerical, have been developed during the last two decades to provide simulation tools. The ability to study and understand nonlinear propagation has become of great importance, especially for military (explosion surveillance, detection) and civil (buildings response) applications.

## 1.1. CSTB

This master's thesis has been carried out in the CSTB establishment of Grenoble (France) from early July to December 2007. CSTB carries out research into a broad range of disciplines and technologies in every field of construction, including the urban environment, health, communications, economics and sociology. The research furthers public policies and makes it possible to develop skills and showcase French engineering in major international projects. In addition to carrying out the basic research required to improve fundamental knowledge, the research teams focus on structural themes and transversal projects. These themes highlight not only problems relating to risks and sustainable development, but also the tools and applications of information and communication technologies. They respond to trends in construction-related trades

towards more management and renovation of real property, in particular via specific multi-disciplinary procedures.

Three main priorities:

- Sustainable development (environmental quality, energy, health). The aim is to provide both public authorities and professionals with the technical, economic and sociological skills required for the elaboration of evaluation methods, decision-making tools, design rules, etc. A large proportion of the work relates to the energy efficiency of buildings with a view to stronger thermal regulations.
- Safety and risks. Strengthening research potential into risks relating to buildings, urban environments and climate change is a response to increasing demand from society.
- Applications and uses of new information and communication technologies (NICTs). This research deals with data processing, the modelling of project information, the management of information flows for the construction sector and property management.

Three transversal projects:

- The virtual laboratory. This project involves the development of simulation tools composed of a range of intercommunicating software and databases, thus making it possible to analyse the performance of building components or parts of building structures.
- The enriched virtual environments platform. This project aims to develop tools to assist in the design of architectural and urban projects and evaluate their performance. It will lead to the development of innovative methods to assist in decision-making (virtual models which can be used for public inquiries), design (cooperative work based on virtual models), or to carry out complex projects (visits to virtual construction sites), etc.
- Existing buildings. The work aims to develop skills relating either to assistance for major contracting authorities and managers of large building stocks or for complex operations. CSTB plays a very active role in EU and international research projects. In addition to its cooperative activities, it submits new research directions to networks to which it belongs, and rallies the most effective organizations to these projects. CSTB chairs several committees in various research networks relating to construction.

To accelerate research processes and broaden the international spectrum of skills, CSTB is developing an active policy of partnerships and exchanges with foreign universities and research centres.

## 1.2. Goals

Numerical codes previously developed at the CSTB don't include nonlinear effects. The main goal of this research period is to develop a tool for nonlinear outdoor sound propagation, so that the propagation of high amplitude waves in a realistic environment can be simulated. The results of such developments can be used for military applications: target detection or nuclear activity monitoring. Another aim is to provide a tool that allows to be used as an input to other methods: the calculation of time signals at a building frontage can be used to study the structure dynamic response to shock wave excitation. Boundary element methods could also be used to design protections to buildings or sensitive structures. A methodology has then to be developed to accomplish this coupling between numerical methods in an efficient way.

## 1.3. Content

Chapter 2 is a review of most areas of nonlinear outdoor sound propagation that are of interest for the control of community noise and/or environmental acoustics. Because the field is so diffuse only the dominant mechanisms are presented. Sections 2.1 to 2.4 present basic principles of wave propagation in a complex environment while section 2.5 introduces the basic principles and fundamental equations of nonlinear acoustics.

Chapter 3 describe the selected numerical model. First a brief state of the art is given in section 3.1 and the choice of the numerical method is explained. Section 3.2 gives in-depth explanations of the governing equations, which implementations are described in section 3.3.

Chapter 4 presents the model validation process. The validation is done in two steps: first nonlinear effects calculations are assessed (section 4.1) and then linear propagation results are compared to another (linear) wave propagation code (section 4.2).

The last chapter (chapter 5) uses all the results obtained to analyze the propagation of a blast wave. A chemical factory called AZF exploded in september 2001 causing many injured and damages in the city of Toulouse (south-west of France). A study performed at the CSTB in 2002 is recast with nonlinear effects included in the model. The coupling of the developed method with a different numerical model is then examined in section 5.3. This work on combining several methods emphasized the need to know *when* nonlinear effects can be neglected in wave propagation. A simple prediction model is developed and described in section 5.4. Finally, conclusion and perspectives to the work accomplished are given in chapter 6.



## 2. Nonlinear outdoor sound propagation

This chapter is a review of most areas of sound propagation outdoors that are of interest for the control of community noise and/or environmental acoustics. Because the field is so diffuse only the dominant mechanisms will be presented here; more detailed information can be found in articles by Embleton [16], Piercy [45] or Ingård [23]. The first two areas covered in this chapter are geometrical spreading (section 2.1) and atmospherical absorption (section 2.2). Together, these are the dominant mechanisms determining the sound levels in sound propagation outdoors. The ground effects are treated in section 2.3 and the meteorological effects in section 2.4. The latter (section 2.5) includes a brief description of nonlinear acoustics and special phenomena, such as wave steepening and shock wave formation, and also presents the main model equations used in nonlinear acoustics.

### 2.1. Geometrical spreading

Waves spread in three dimensions when the sound source is small compared to the distances being considered. The resulting attenuation depends on the propagation distance, and is frequency independent. For a spherical sound source in an homogenous medium in free field, the acoustic power is uniformly spread on a spherical wavefront. The wavefront area being proportional to the square of the sphere radius, the acoustic intensity decays by  $1/R$  and the acoustic pressure by  $1/R^2$ . At twice the distance from the source, the wavefront area is four times as large, and sound pressure levels decrease by 6 dB. Each time the distance is doubled, the sound pressure levels decrease by 6 dB. Sound waves spread cylindrically from a line of sources which are all similar but radiate independently. The area of the cylindrical wavefront is proportional to the distance, the sound pressure level thus decreases by 3 dB per doubling of distance, at half the rate of spherical spreading (see Figure 2.1).

### 2.2. Atmospherical absorption

Atmospheric absorption is a feature of wave propagation that is always present in outdoor sound propagation. Although it may be neglected in some applications, this phenomena has to be carefully taken care of in long-range propagation. The global absorp-

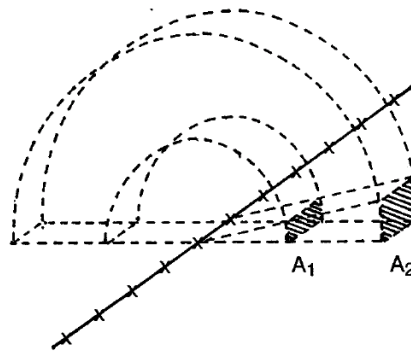


Figure 2.1.: Schematic diagram for cylindrical spreading. Area  $A$  of cylindrical wavefronts is proportional to the distance  $d$  from the line of sources,  $A_2 = 2A_1$  when  $d_2 = 2d_1$ . Sound pressure levels decrease by 3 dB per doubling of distance. This Figure is taken from Piercy [45].

tion phenomenon is mainly due to three physical effects:

- Classical absorption caused by the transport processes of classical physics (shear viscosity, thermal conductivity, mass diffusion and thermal diffusion).
- Rotational relaxation of molecules in air.
- Vibrational relaxation of molecules of oxygen and nitrogen.

The atmospheric absorption due to the different physical effects is shown on Figure 2.2. Note that the attenuation by absorption is constant for a given *difference* in propagation path lengths unlike geometrical spreading, where it is constant for a given *ratio* of propagation path lengths. Thus attenuation tends to be more and more important with increasing distance between source and receiver. This Figure also shows the frequency dependency of the absorption coefficient: the sound attenuation is more and more important as the frequency increases; only low frequency noise are able to propagate through large distances.

### 2.3. Features due to the ground

In this section the different roles of the ground in sound propagation are detailed. First the case of sound reflexions on a flat, rigid ground and the resulting interference pattern is detailed (section 2.3.1). The second section (section 2.3.2) deals with the case of non-rigid ground; different impedance models are quickly reviewed. Propagation

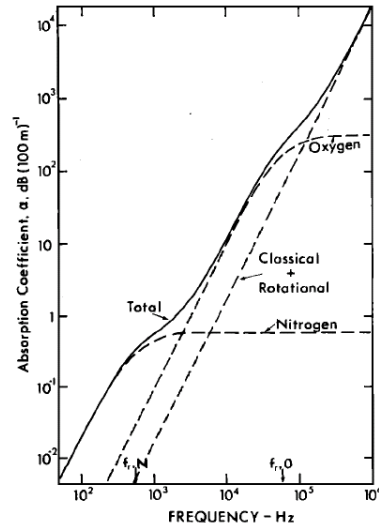


Figure 2.2.: Atmospheric absorption in dB/100 m for a pressure of 1 atm, temperature of 20 °C and relative humidity of 70 %. This Figure is taken from Piercy [45].

through city streets, attenuation due to barriers and in general, propagation over terrain with complex topography are excluded; these subjects would require a lot of time to be treated in detail.

### 2.3.1. Path-length differences (PLD)

When both the source and receiver are above the ground a phase change occurs due to the different lengths of direct and reflected waves paths. This phase change occurs in addition to the change due to the ground characteristic, but we'll consider here the ground totally rigid so that PLD effects can be studied (see Figure 2.3 for a schematic of the configuration). Provided the grazing angle  $\psi$  is small, the path-length difference between direct and reflected wave can be calculated with the formula:

$$PLD \approx 2h_s h_r / d$$

The effect of path-length difference is a cancellation of pressure at the receiver for PLD's of an odd numbers of half-wavelengths. Some examples of measured excess attenuation spectra are shown in Figure 2.4.

### 2.3.2. Ground impedance

The reflection coefficient for a plane wave on a locally reacting surface is:

$$R_p = \frac{\sin(\psi) - Z_1/Z_2}{\sin(\psi) + Z_1/Z_2}$$

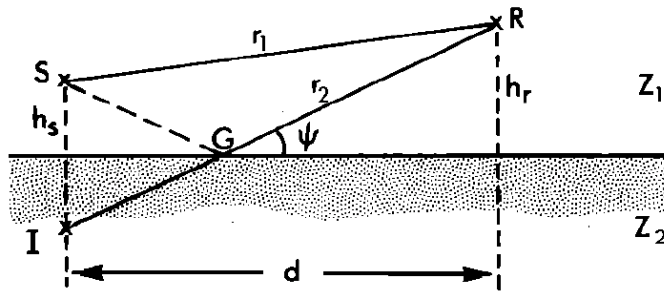


Figure 2.3.: Reflection of sound on a flat ground. This Figure is taken from Piercy [45].

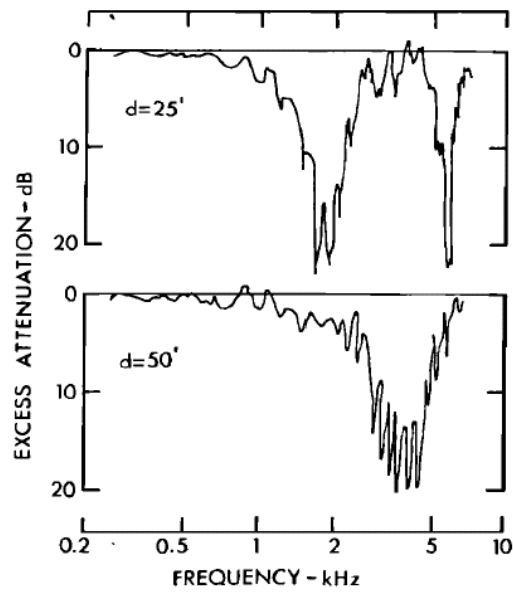


Figure 2.4.: Measured excess attenuation for propagation from a point source over asphalt,  $h_s = 0.3$  m,  $h_r = 1.2$ . This Figure is taken from Piercy [45].

where  $\psi$  is the grazing angle,  $Z_1 = \rho c$  is the characteristic impedance of air and  $Z_2$  is the acoustic impedance of the surface. The acoustic characteristics of a locally reacting surface may be represented by its acoustical impedance  $Z_2 = R_2 + jX_2$ . This impedance value may depend on the frequency but not on the grazing angle. The hypothesis of a locally reacting ground has been proven to be valid for most of the surface used in outdoor sound propagation (see for example the article by Attenborough [4] or the book by Salomons [49]). Attenborough, Bérenghier, Delany and Bazley, Biot or Allard developed different impedance models which validity depends on the frequency and the material considered. They are based on different theoretical models and differ by their complexity. The Delany and Bazley model is presented here; it is an empirical model that allow to model absorbing fibrous materials. The expression of the normalized impedance for a material of flow resistivity  $\sigma$  is:

$$Z_2 = 1 + 9.8 \left( \frac{f}{\sigma} \right)^{-0.75} + j11.9 \left( \frac{f}{\sigma} \right)^{-0.73}$$

Although this model is simple –the impedance only depends on the frequency and the flow resistivity– it has been shown that the results obtained are in good agreement with the measurements. This model is commonly used in outdoor sound propagation. Note that for low frequencies, the ground impedance absolute value becomes very high and thus, the reflection coefficient is close to unity (rigid ground).

## 2.4. Meteorological effects

In this section the meteorological conditions usually encountered in outdoor sound propagation are described (section 2.4.1) and their effects on wave propagation is detailed in section 2.4.2.

### 2.4.1. Relevant meteorological phenomena

The complete meteorological description of an environment is a complex task: a lot of quantities such as temperature, wind velocity, air density, air pressure, turbulences, intervene in this description. These values are obviously not independant and most of the time vary in time and space. Taking into account all of these parameters in a numerical model is a work that can't be done here. Nevertheless, from an acoustician point of view, we can denote two dominant parameters that will modify sound propagation paths: wind speed and temperature gradients. These two quantities locally affect the *effective* sound celerity and thus change the way sound propagates.

### Temperature gradients

During the daytime the variation of temperature with height for a large flat area may be represented by the expression:

$$T = T_0 - K_t \log(z/z_0) \quad (2.1)$$

where  $T_0$  is the temperature for  $z \leq z_0$ . During night the ground surface will cool due to radiation to the air. This phenomena is known as an inversion; examples of such temperature profiles are shown in Figure 2.5.

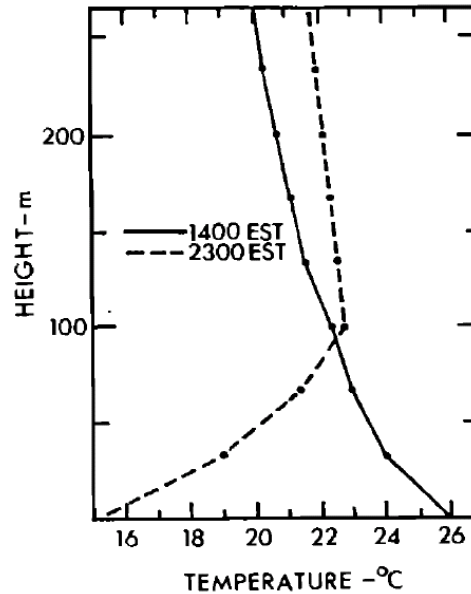


Figure 2.5.: Variation of temperature; examples of lapse and inversion conditions. This Figure is taken from Munn [41].

### Wind velocity gradients

Wind velocity is a three-dimensional vectorial quantity difficult to represent due to its spatial and temporal instability. The variation of the average windspeed  $V$  with height  $z$  in the vicinity of the ground for a flat area is approximately as shown in Figure 2.6. This speed profile may be represented with a logarithmic law; for altitudes greater than  $z_0$  the wind speed can be expressed by:

$$V = K_v \log(z/z_0) \quad (2.2)$$

Parameter  $z_0$  is determined by the roughness of the surface, and is often approximately the height of a consistent obstacle. The constant  $K_v$  is determined by the roughness

of the surface and the wind velocity above this layer. If we neglect the vertical component of the wind speed (which is often very small in comparison to the horizontal component), we can write the sound speed with the following formula:

$$c(x, z) = c_0 + \|\overrightarrow{V(x, z)}\| \approx c_0 + V_x$$

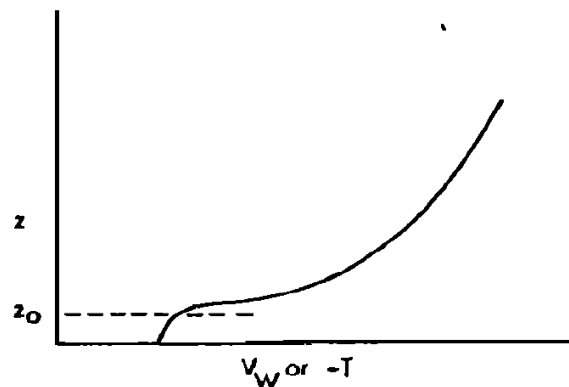


Figure 2.6.: Variation of wind velocity and temperature in the vicinity of a flat ground surface. This Figure is taken from Piercy [45].

### 2.4.2. Refraction

The wave celerity variations with the altitude will be responsible for a phenomena called refraction. Refraction caused by wind and temperature variations are different: temperature is a scalar quantity, and thus the refraction will be identical in all horizontal (compass) directions. However, the refraction caused by wind depends on the sound direction of propagation. If the sound propagates directly crosswind, the refraction from wind is zero, and increases progressively as the direction of propagation deviates from its direction. Two types of refraction can be denoted: downwards and upwards refraction.

#### Downwards refraction

Downwards refraction occurs when the sound speed increases with the altitude: the sound field curves downwards as shown in Figure 2.7. If the source and receiver are both above the ground, downward refraction will cause multiple reflections on the ground (see Figure 2.8). This phenomena has two consequences: amplifying the ground effects and increasing the pressure at the receiver.

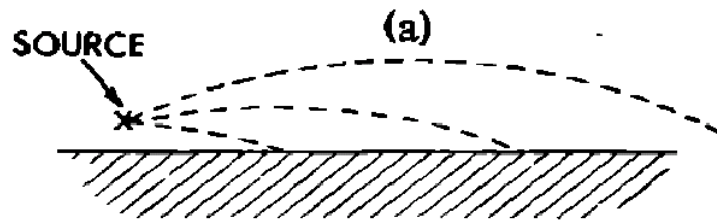


Figure 2.7.: Schematic diagram for a downwind situation. This Figure is taken from Piercy [45].

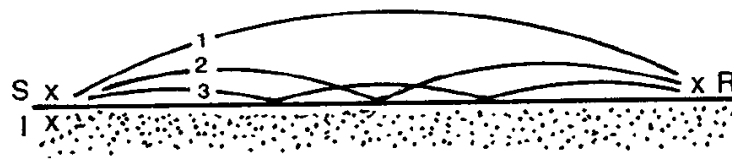


Figure 2.8.: Multiple reflections resulting from a downwind situation described in Figure 2.7. This Figure is taken from [16].

### Upwards refraction

Upwards refraction occurs, at the opposite, when the sound speed is decreasing with altitude, typically at daytime. If the source and receiver are above the ground the sound rays will be bent upwards. This will create a shadow zone where the pressure will be zero; the ray delimiting this area is tangent to the ground surface (see Figure 2.9).

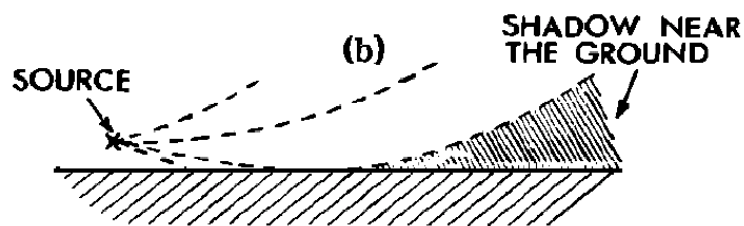


Figure 2.9.: Schematic diagram for an upwind situation. This Figure is taken from Piercy [45].

## Complex situations

Combined effects of temperature and wind gradients can lead to very complex situations where sound ray paths can adopt various trajectories. Below are presented two cases taken from the article by Ingård [23] which describe complex situations that can be found in outdoor sound propagation.

**First case (see Figure 2.10)** In this particular case there is a change of wind gradient at the layer 3 km above the ground. Above this layer the wind gradient can no longer compensate for the temperature gradient, and the rays will all be bent upwards in this region. The rays in the vertical plane in the wind direction are shown to reach out to a distance of 38.8 km from the source. Beyond this distance there will be a shadow zone.

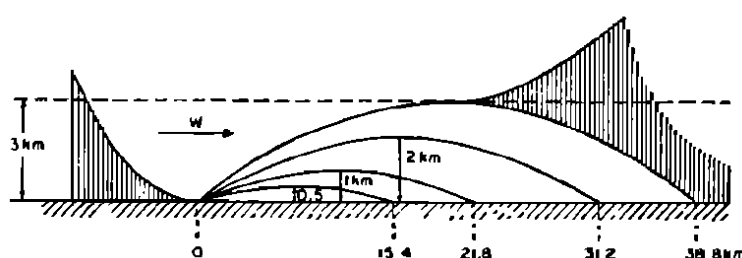


Figure 2.10.: Illustration of a combined effects of temperature and wind (case 1). This Figure is taken from Ingård [23].

**Second case (see Figure 2.11)** In this different configuration the wind gradient is everywhere the same except in a thin layer located 1 km above the ground. The velocity jumps here from a value  $u_1$  to  $u_2$  and the sound rays are refracted as shown. The ray that is tangent to the layer at a height of 1 km represents the limiting ray for the first audible region. Rays with larger angles of elevation will enter the second layer and thus be bent downwards to form a second audible region, as shown in Figure 2.11.

## 2.5. Nonlinear acoustics

This section introduces the basic principles and fundamental equations of nonlinear acoustics; the reader may refer to two books by Enflo and Hedberg [17] or Blackstock and Hamilton [20] for complete information on the topic. Since long time ago it has been known that there are acoustical phenomena that cannot be described by linear acoustic. In fact the condition for linear acoustics to be applicable is that the amplitude

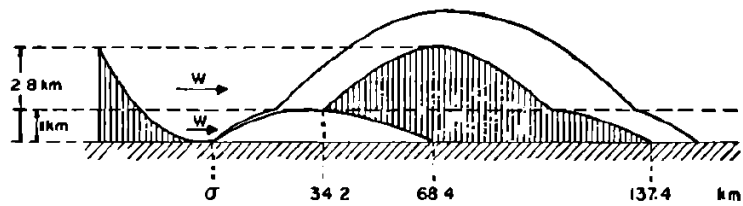


Figure 2.11.: Illustration of a combined effects of temperature and wind (case 2). This Figure is taken from Ingård [23].

of the sound wave is sufficiently small; finite amplitude sound must be described by nonlinear acoustics. Nonlinear acoustics began its development as a specialty within the science of acoustic as late as in the middle of the twentieth century.

The fundamental problem of deformation and decay of a sine-wave has been investigated during the 60's. This phenomena comes from the fact that the wave celerity is no more independant of the wave properties. Indeed, the wave speed depends on the particle velocity amplitude. As the amplitude grows, the wave celerity increases (and vice-versa). This is an accumulative process and it increases when the wave proceeds; it means that even a relatively weak wave can steepen into a shock (provided losses are not significant).

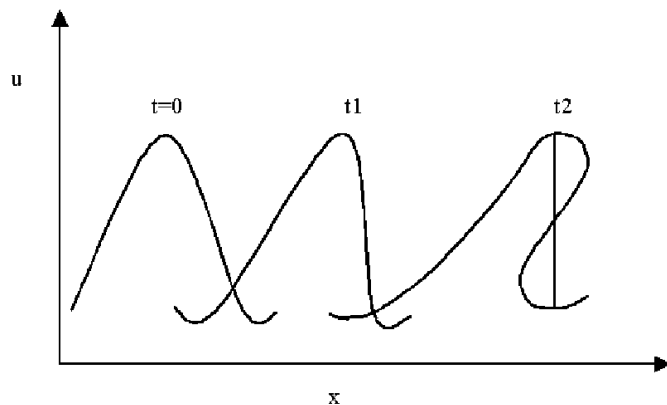


Figure 2.12.: Wave deformation and decay.

### 2.5.1. Wave equations of nonlinear acoustics

In this section, three fundamental equations of nonlinear acoustics are presented: these are the Fubini's solution, the Burgers equation and the KZK equation. These three equations differ by their complexity and their field of application.

### Fubini's solution

Fubini developed a solution for the nonlinear propagation of monofrequency sources. This solution is valid *only before* the shock formation. The pressure distribution is expressed by an infinite sum of weighted Bessel functions:

$$p(\sigma, \tau) = p_0 \sum_{n=1}^{\infty} \frac{2}{n\sigma} J_n(n\sigma) \sin(n\omega\tau) \quad (2.3)$$

where  $\sigma = x/\bar{x}$ ,  $\tau = t - x/c_0$ ,  $p_0$  is the initial sinusoid amplitude and  $J_n$  is the Bessel function of order  $n$ .  $\bar{x}$  is the shock formation distance; as said before, equation 2.3 is valid for  $\sigma < 1$ , in the pre-shock region. The Fubini's solution is fast and easy to implement and solve, but this formulation cannot handle complex problems:

- The solution is valid only before the shock formation.
- Losses can't be included in the model.
- The model gives solutions for 1D problems only.

Figure 2.13 presents the deformation and decay of a sine wave calculated with the Fubini's solution.

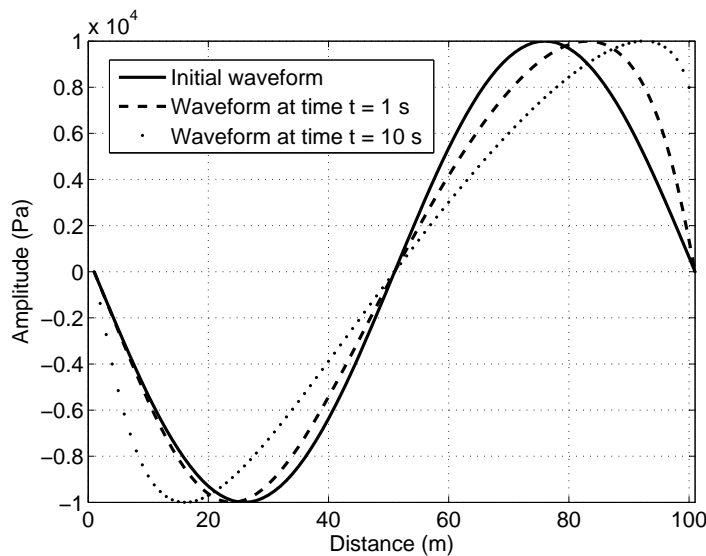


Figure 2.13.: Deformation of a sine-wave calculated with the Fubini's solution.

### The Burgers equation

The Burgers equation is the simplest model that properly describes the combined effects of nonlinearity and losses on the propagation of plane progressive waves. The Burgers

equation is:

$$\frac{\partial p}{\partial x} - \frac{\zeta}{2c_0^3} \frac{\partial^2 p}{\partial \tau^2} = \frac{\beta}{2\rho_0 c_0^3} \frac{\partial p^2}{\partial \tau} \quad (2.4)$$

where  $\zeta$  is the sound diffusivity, a parameter that accounts for dissipation (see section 3.2.4 page 25 for a detailed definition).  $\tau = t - x/c_0$  represents a retarded time frame, *i.e.* a reference frame moving at speed  $c_0$ , and  $\beta = \frac{\gamma+1}{2}$  is the nonlinearity coefficient of the medium ( $\gamma$  is the ratio of specific heat at constant volume and pressure).

Equation 2.4 is the most widely used equation model for studying the combined effects of dissipation and nonlinearity on progressive plane waves. The above equation can be extended to handle divergence (or convergence) of progressive spherical or cylindrical waves. This new equation, the *generalized Burgers equation*, allows to consider more configurations and in the case of plane waves, reduces to equation 2.4.

### The KZK equation

The KZK (Khokhlov-Zabolotskaya-Kuznetsov) equation is an augmentation of the Burgers equation presented in section 2.5.1 that accounts for the effects of diffraction, absorption and nonlinearity for directional sound beams. The KZK equation is:

$$\frac{\partial^2 p}{\partial z \partial \tau} - \frac{c_0}{2} \nabla_{\perp}^2 p - \frac{\zeta}{2c_0^3} \frac{\partial^3 p}{\partial \tau^3} = \frac{\beta}{2\rho_0 c_0^3} \frac{\partial^2 p^2}{\partial \tau^2} \quad (2.5)$$

where  $z$  is the beam propagation direction,  $\nabla_{\perp}^2 = \partial^2/\partial x^2 + \partial^2/\partial y^2$  is a Laplacian that operates in the plane perpendicular to the axis of the beam. Note that in the absence of diffraction ( $\nabla_{\perp}^2 p = 0$ ) equation 2.5 reduces to the Burgers equation (equation 2.4).

## 3. Computational method

In this section the computational method chosen is described. First a brief state of the art is given in section 3.1 and the choice of the model is explained. Section 3.2 gives in-depth explanations of the governing equations, which implementations are described in section 3.3.

### 3.1. State of the art

Numerical simulations in acoustics benefit from a large panel of different methods, which greatly differ by their complexity, but the choice is restricted for nonlinear propagation in complex environments. The selected method will have to:

- Recreate nonlinear effects (at least weak nonlinearities).
- Accurately simulate absorption from air.
- Allow the use of spatially varying quantities (such as temperature or wind velocity).
- Solve the problem in a two dimensional space in a reasonable amount of time (possibly extendable to 3D configurations).

Although the ability to handle non-rigid grounds and complex topographies can be of great interest in outdoor sound propagation, these features have not been retained as being determinant in the choice of the numerical method. The assumption of rigid ground is to be balanced by the context of numerical simulations: explosions produce broad-band signals, but the wave will propagate over several kilometers. For the distances considered, the high-frequency content of the signal will be attenuated quickly by atmospherical absorption, and for very low frequencies, the reflection coefficient is often close to unity. The calculation time required by the calculation is a crucial parameter: although computational power considerably increased during the last two decades, it is still a determinant parameter in the choice of a numerical method. Two different methods are commonly used to solve for such problems; these are:

1. General time domain algorithms (see section 3.1.1).

2. Time domain algorithms based on the nonlinear progressive wave equation (NPE) (see section 3.1.2).

Complete information and references about these methods can be found in the book by Hamilton and Blackstock [20].

### 3.1.1. General time domain algorithm

Pierce [44] derived a set of equations inspired by fluid dynamics for nonlinear sound propagation. The fluid dynamic equations that govern the wave propagation are the continuity equation, the Navier-Stokes equation (momentum equation), the entropy balance equation and the relaxation equation. The latest developed models (see Wochner [60] or Sparrow [52]) are very complete: a lot of features from outdoor sound propagation can be included. The numerical model established by Wochner [60] can recreate nonlinear phenomena accurately, simulate absorption and dissipation<sup>1</sup>, and represent realistic atmospheric conditions (spatially varying quantities). The equations derivation leads to a system of differential equations which can be written with the time derivatives of the constitutive equations in the  $\mathbf{w}$  vector, the  $x$  derivatives in the  $\mathbf{F}$  vector, the  $y$  derivatives in the  $\mathbf{G}$  vector, and the source terms in  $\mathbf{H}$ .

$$\frac{\partial \mathbf{w}}{\partial t} + \frac{\partial \mathbf{F}}{\partial x} + \frac{\partial \mathbf{G}}{\partial y} = \mathbf{H} \quad (3.1)$$

where

$$\mathbf{w} = \begin{pmatrix} \rho \\ \rho u \\ \rho v \\ \rho s_{fr} \\ \rho T_{N_2} \\ \rho T_{O_2} \end{pmatrix}, \mathbf{F} = \begin{pmatrix} \rho u \\ \rho u^2 \\ \rho uv \\ \rho us_{fr} \\ \rho u T_{N_2} \\ \rho u T_{O_2} \end{pmatrix}, \mathbf{G} = \begin{pmatrix} \rho v \\ \rho uv \\ \rho v^2 \\ \rho vs_{fr} \\ \rho v T_{N_2} \\ \rho v T_{O_2} \end{pmatrix}$$

and

$$\mathbf{H} = \begin{pmatrix} 0 \\ -\frac{\partial p}{\partial x} + \mu_B \left( \frac{\partial^2 u}{\partial x^2} + \frac{\partial^2 v}{\partial x \partial y} \right) + \mu \left( \frac{\partial \Phi_{xx}}{\partial x} + \frac{\partial \Phi_{xy}}{\partial y} \right) \\ -\frac{\partial p}{\partial y} + \mu_B \left( \frac{\partial^2 v}{\partial y^2} + \frac{\partial^2 u}{\partial y \partial x} \right) + \mu \left( \frac{\partial \Phi_{yx}}{\partial x} + \frac{\partial \Phi_{yy}}{\partial y} \right) \\ \sigma_s - \sum_v \frac{\rho}{T_v} C_{vV} \frac{DT_v}{Dt} + \nabla \cdot \left( \frac{\kappa}{T} \nabla T \right) \\ \frac{\rho}{\tau_{N_2}} (T - T_{N_2}) \\ \frac{\rho}{\tau_{O_2}} (T - T_{O_2}) \end{pmatrix}$$

<sup>1</sup>Due to shear viscosity and Bulk viscosity, thermal conductivity, and molecular relaxation processes.

In the above equation,  $\rho$  is the density,  $t$  the time,  $u$  and  $v$  the component of the velocity vector,  $p$  the pressure,  $\mu$  and  $\mu_B$  the shear and Bulk viscosity,  $\Phi$  the rate of shear tensor,  $s_{fr}$  the frozen entropy,  $T$  the absolute temperature,  $\kappa$  the coefficient of thermal conduction,  $c_{vv}$  the specific heat at constant volume associated with the  $v$ -type molecule,  $\sigma_s$  a variable used to represent the source terms, and  $T_v$  and  $\tau_v$  the apparent vibration temperature and relaxation time of the  $v$ -type molecule, respectively. Equations in the form of equation 3.1, in which all of the variables on the left hand side are within the derivative operators of  $t$ ,  $x$ , or  $y$ , may be solved by many explicit finite-difference approximations.

Although the numerical model presented above leads to very accurate solutions for nonlinear sound propagation, the computational time needed makes it difficult to use for long-range propagation. A convenient resolution for acoustic waves is 20 points/ $\lambda$ ; a frequency of 20 Hz leads to maximum spatial steps of 0.85 meters. Simulating the propagation of this wave over a domain which is 10 km wide and 2 km high would result in a grid which contains more than 27 billion points! Grids of this size can't be managed on a "simple" workstation. Several methods exist to lower the numerical effort: adaptive mesh refinement (AMR) techniques rely on the principle that it is not necessary to mesh *the entire* grid. These kind of numerical methods would be well adapted to the problems envisaged: since finite-length signals are considered only a small area around the wavefront would *have* to be meshed. The implementation of such algorithms is a very complex task that can't be done in the framework of this master's thesis.

### 3.1.2. Time domain algorithm based on the NPE

Nonlinear progressive wave equation (NPE) is a time domain approach used to model finite amplitude sound waves propagation in complex environments. This method has first been developed by McDonald and Kuperman [39] in 1987 and has been successfully used for underwater acoustics simulations (see for example McDonald [54]). The method can be adapted to simulate the propagation of high-amplitude signals through air. Indeed, in its original formulation the NPE cannot be used to accurately simulate atmospherical propagation: features like geometrical decay and thermoviscous effects need to be added. These modifications, described in several articles, lead to a new, augmented equation, which is able to simulate propagation through a complex atmosphere.

The NPE is a kind of simplification of the Euler equation finite difference model. Its fundamental principle is the calculation of the wave evolution in a "moving window", and not over the complete physical domain (see Figure 3.1 for a schematic). A moving grid that surrounds the signal moves at speed  $c_{win}$ , and the wave evolution is calculated *within* the window. The results are post-processed to get back to the *physical* wave

movements.

The main advantage of such method is the reduced computational time: the mesh is just wide enough to contain the signal, thus avoiding to mesh several kilometers for the whole domain. This imply some restrictions:

1. As the wave is calculated over a window surrounding it, only finite-length signals can be used. Stationary conditions can't be simulated.
2. The method simulate propagation in only one direction. Back-propagation, for example in case of an obstacle, can't be taken into account.

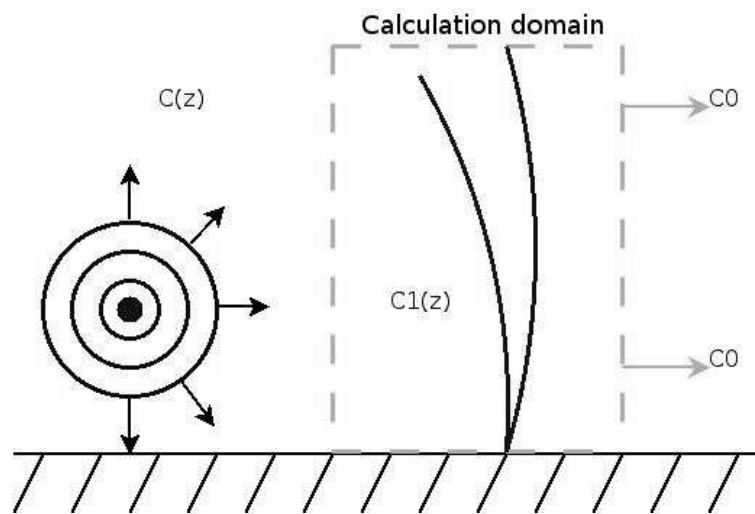


Figure 3.1.: The wave-following NPE grid moves at speed  $c_0$  in the  $r$  direction to integrate nonlinear wave evolution in the time domain.

These two restrictions are in accordance with the type of simulations considered: signals are finite in length, and one-way propagation is a good assumption for long-rangesimulations.

Although the nonlinear progressive wave equation is restricted to one-way, finite-length signals propagation it is totally adapted to explosion-type signals modelisation. By adding geometrical spreading and thermoviscous effects (absorption and dissipation) to the original NPE, nonlinear atmospherical propagation can be accurately simulated by the method.

### 3.2. The nonlinear progressive wave equation

This chapter presents the selected numerical model: the original formulation is first given and additional features (geometrical spreading, thermoviscous effects, high-angle

formulation are then detailed to lead to a new, augmented NPE.

### 3.2.1. Derivation and original formulation

In this section the derivation of the constitutive equations that lead to the original nonlinear progressive wave equation (NPE) formulation is recast in a cartesian, two-dimensional coordinates system. The aim of this section is to provide the reader the theoretical background and foundations of the NPE; the derivation is taken from a reference article by McDonald and Kuperman [39] (similar derivations can be found in other references such as Caine [7][11] or James [26]).

The cartesian formulation of the continuity equation is:

$$\frac{\partial \rho_T}{\partial t} + \frac{\partial}{\partial x} (\rho_T u) + \frac{\partial}{\partial y} (\rho_T v) = 0 \quad (3.2)$$

where the flow velocity vector is  $U = (u, v)$ . The quantity  $\rho_T$  is a total variable ; it includes the density of air at rest *and* the acoustic density perturbation, so that:  $\rho_T = \rho_0 + \rho$ . We assume here an irrotational flow in the y-axis direction (the main propagation direction is along the x-axis); this allows to get an expression for the y-component of the flow velocity vector:

$$v = \int \frac{\partial u}{\partial y} dx \quad (3.3)$$

Replacing the total quantity  $\rho_T$  by  $\rho_0 + \rho$ , equation 3.2 becomes:

$$\frac{\partial \rho}{\partial t} + \frac{\partial}{\partial x} ((\rho_0 + \rho) u (\rho_0 + \rho)) + \frac{\partial}{\partial y} \left( (\rho_0 + \rho) \int g(\rho_0 + \rho) \frac{\partial \rho}{\partial y} dx \right) = 0 \quad (3.4)$$

with:

$$g(\rho_0 + \rho) = \frac{du(\rho_0 + \rho)}{d\rho} \quad (3.5)$$

Note that only two hypotheses are made to get equation 3.4:

1.  $u$  is a function of  $\rho_T$ .
2. The flow is irrotational in the transverse propagation direction.

One has now to determine an expression for the quantity  $u = u(\rho_T)$ ; the momentum equation along the x-axis is used:

$$\frac{\partial (\rho_T u)}{\partial t} + \frac{\partial}{\partial x} (p_T + \rho_T u^2) + \frac{\partial}{\partial y} (\rho_T u v) = 0$$

Integrating with respect to time leads to an expression for  $\rho_T u$ :

$$\rho_T u = - \int \left[ \frac{\partial}{\partial x} (p_T + \rho_T u^2) + \frac{\partial}{\partial y} (\rho_T u v) \right] dt \quad (3.6)$$

Inserting equations 3.6 and 3.3 in 3.4 gives:

$$\begin{aligned} \frac{\partial \rho_T}{\partial t} - \frac{\partial}{\partial x} \left\{ \int \left[ \frac{\partial}{\partial x} (p_T + \rho_T u^2) + \frac{\partial}{\partial y} \left( \rho_T u + \left( \int \frac{\partial u}{\partial y} dx \right) \right) \right] dt \right\} \\ + \frac{\partial}{\partial y} \left( \rho_T \left( \int \frac{\partial u}{\partial y} dx \right) \right) = 0 \end{aligned} \quad (3.7)$$

The last term in equation 3.7 is associated with the diffraction term in the y-axis direction. The pressure  $p_T$  and the flow velocity component  $u$  are now developed with Taylor series:

$$\begin{aligned} p_T &= p(\rho_0) + \left( \frac{\partial p}{\partial \rho} \right)_0 (\rho_T - \rho_0) + \frac{1}{2} \left( \frac{\partial^2 p}{\partial \rho^2} \right)_0 (\rho_T - \rho_0)^2 + \dots \\ u &= \left( \frac{\partial u}{\partial \rho} \right)_0 (\rho_T - \rho_0) + \frac{1}{2} \left( \frac{\partial^2 u}{\partial \rho^2} \right)_0 (\rho_T - \rho_0)^2 + \dots \end{aligned} \quad (3.8)$$

To the first order, equation 3.8 becomes:

$$u = \frac{c}{\rho_0} \rho$$

The next step is to insert this expression into equation 3.5:

$$g = \frac{c}{\rho_0}$$

These operations let equation 3.7 be transformed:

$$\frac{\partial \rho_T}{\partial t} - \frac{\partial}{\partial x} \left\{ \int \frac{\partial}{\partial x} (p_T + \rho_T u^2) dt \right\} + c \frac{\partial^2}{\partial y^2} \left\{ \int \rho dx \right\} = 0 \quad (3.9)$$

It is important to note that the diffraction operator  $c \frac{\partial^2}{\partial y^2} \left\{ \int \rho dx \right\}$  is developed to the first order only. The integral in the above equation can be removed by differentiating 3.9 with respect to time.

$$\frac{\partial^2 \rho}{\partial t^2} - \frac{\partial^2}{\partial x^2} (p_T + \rho_T u^2) + c \frac{\partial^2}{\partial y^2} \left( \int \frac{\partial \rho}{\partial t} dx \right) = 0 \quad (3.10)$$

One can now use the linearized momentum equation to simplify equation 3.10:

$$\frac{\partial^2 \rho}{\partial t^2} - \frac{\partial^2}{\partial x^2} (p_T + \rho_T u^2) - c^2 \frac{\partial^2 \rho}{\partial y^2} = 0 \quad (3.11)$$

An important remark has to be done at this stage: the classical (linear) wave equation can easily be derived from equation 3.11. If the ambient medium pressure is constant then  $p_T = p = c^2 \rho$  (linear case), and if high order terms are neglected one gets:

$\frac{\partial^2 \rho}{\partial t^2} - c^2 \nabla^2 \rho = 0$ , which is the well-known wave equation.

A one-way propagation has now to be assumed, i.e. there is no backward propagation. Although this hypothesis is quite restrictive, it is well adapted to long-rangesound propagation. Thanks to this new assumption equation 3.11 can be expressed in a moving window, which speed is  $c_{win}$ , a value close to the wave celerity at rest. A new “moving window” operator is introduced:

$$\frac{D}{Dt} = \frac{\partial}{\partial t} + c_{win} \frac{\partial}{\partial x} \quad (3.12)$$

where  $c_{win}$  is the window celerity. Assuming spatially-varying sound celerity  $c(x, y)$ ,  $c_{win}$  is defined by:

$$c_{win} = \max(c(x, y)) \quad (3.13)$$

With this moving window celerity, the sound speed perturbation *in the window*  $c_1(x, y) = c_{win} - c(x, y)$  becomes negative. Indeed, the NPE can only propagate the signal in one direction; the wave front evolves backward *in the window*, but propagates forward in the entire domain. It can be proved that  $D_t^2 \rho \simeq 0$  (see for example Caine [11]); one then gets:

$$\frac{\partial^2 \rho}{\partial t^2} = -2c \frac{\partial^2 \rho}{\partial x \partial t} - c^2 \frac{\partial^2 \rho}{\partial x^2}$$

And equation 3.11 becomes:

$$\frac{\partial^2 \rho}{\partial x \partial t} + \frac{1}{2c} \frac{\partial^2}{\partial x^2} [p_T + \rho_T u^2 + c^2 \rho] + \frac{c}{2} \frac{\partial^2 \rho}{\partial y^2} = 0 \quad (3.14)$$

So that a second order accuracy can be retained in equation 3.14,  $p_T$  is transformed with the help of expression 3.8 with the derivatives coefficients corresponding to an isentropic flow:  $\left(\frac{\partial p}{\partial \rho}\right)_0 = c^2$  and  $\left(\frac{\partial^2 p}{\partial \rho^2}\right)_0 = \frac{c^2}{\rho_0} (\gamma - 1)$  where  $\gamma$  is the ratio of specific heats at constant pressure and volume. One gets the following equations:

$$p_T \simeq p_0 + c^2 \rho + \frac{1}{2} \frac{(\gamma - 1) c^2}{\rho_0} \rho^2$$

$$u \simeq c \frac{\rho}{\rho_0} \quad (3.15)$$

Terms of order higher than two are neglected in the bracketed expression; this leads to a new formulation for equation 3.14:

$$\frac{\partial^2 \rho}{\partial x \partial t} + \frac{1}{2c} \frac{\partial^2}{\partial x^2} \left[ 2c^2 \left( \rho + \frac{\beta \rho^2}{2\rho_0} \right) \right] + \frac{c}{2} \frac{\partial^2 \rho}{\partial y^2} = 0$$

For gazes, the coefficient of nonlinearity is calculated with the help of the ratio of specific heat at constant volume and pressure  $\gamma$ :  $\beta = (\gamma + 1) / 2$  and is approximately equal

to 1.2 for air under normal conditions. Applying the replacements above in equation 3.14 and integrating with respect to  $x$  let one finally get an expression for the NPE in a two-dimensional cartesian coordinates system:

$$\frac{D\rho}{Dt} + \frac{\partial}{\partial x} \left( c\rho + c\frac{\beta}{2\rho_0}\rho^2 \right) + \frac{c}{2} \frac{\partial^2}{\partial y^2} \left( \int \rho dx \right) = 0 \quad (3.16)$$

The final step is to replace the density  $\rho$  by the dimensionless variable  $R = \frac{\rho}{\rho_0}$  to get a simpler formulation:

$$\frac{DR}{Dt} + \frac{\partial}{\partial x} \left( cR + c\frac{\beta}{2}R^2 \right) + \frac{c}{2} \frac{\partial^2}{\partial y^2} \left( \int R dx \right) = 0 \quad (3.17)$$

The wave celerity  $c$  may be spatially varying; with this assumption the equation 3.17 can be replaced by:

$$\frac{DR}{Dt} + \frac{\partial}{\partial x} \left( c_1R + c_0\frac{\beta}{2}R^2 \right) + \frac{c_0}{2} \frac{\partial^2}{\partial y^2} \left( \int R dx \right) = 0 \quad (3.18)$$

The equation above is the original formulation of the nonlinear progressive wave equation. It will be later referred to as the *original NPE*. This equation contain three different terms accounting for three different effects in nonlinear outdoor sound propagation:

- The term:  $\frac{\partial}{\partial x} (c_1R)$  takes into account refraction effects; it allows the signal to be propagated *within the moving window*.
- The term:  $\frac{\partial}{\partial x} \left( c_0\frac{\beta}{2}R^2 \right)$  takes into account nonlinear effects; wave steepening and shock formation are calculated with this operator.
- The term:  $\frac{\partial^2}{\partial y^2} \left( \int R dx \right)$  takes into account the diffraction effects, which can be seen as a propagation operator in the transverse direction.

From these previous notes about the operators follows an important remark: geometrical spreading and thermoviscous effects (atmospheric absorption) are not included in this formulation of the NPE.

### 3.2.2. Cylindrical coordinates formulation

A formulation of the NPE for azimuthally symmetric configurations is more adapted to the kind of problems considered. A derivation for cylindrical coordinates system can be found in another article by McDonald [38]. The nonlinear progressive wave equation expressed in a cylindrical coordinate system is:

$$\frac{\partial R}{\partial t} + \frac{c_0}{2} \frac{R}{r} + \frac{\partial}{\partial r} \left( c_1R + c_0\frac{\beta}{2}R^2 \right) + \frac{c_0}{2} \frac{\partial^2}{\partial y^2} \left( \int R dr \right) = 0 \quad (3.19)$$

In the above equation  $r$  is the distance from the vertical axis:  $r = x + c_{win}t$ , where  $x$  is the position inside the window. The equation 3.19 is very similar to the original NPE (equation 3.18 in section 3.2.1): a cylindrical decay term  $\frac{c_0 R}{2 r}$  has been added to the original equation.

### 3.2.3. High-angle formulation

A high-angle formulation of the original NPE has been derived by McDonald [38] in 2000. This new formulation allows to get a better accuracy at high propagation angle close to the source. This is made possible by taking into account into the diffraction operators the terms that are of order two. It is important to note that this development to higher orders only concerns the diffraction operator *and not the nonlinear operator*. The nonlinearities are still taken to the first order.

$$\frac{\partial R}{\partial t} + \frac{c_0 R}{2 r} + \frac{\partial}{\partial r} \left( c_1 R + c_0 \frac{\beta}{2} R^2 \right) + \int \left\{ \frac{c_0}{2} \frac{\partial^2 R}{\partial y^2} + c_0 \frac{R}{r^2} - \frac{1}{2c_0} \frac{D^2 R}{Dt^2} \right\} dr = 0 \quad (3.20)$$

This equation differs from 3.18 by the addition of two terms in the integral.

### 3.2.4. Thermoviscous effects

In its original formulation, the NPE does not take into account the atmospherical absorption. This has been later included by Too and Lee [54]; the new equation is:

$$\frac{\partial R}{\partial t} + \frac{c_0 R}{2 r} + \frac{\partial}{\partial r} \left( c_1 R + c_0 \frac{\beta}{2} R^2 \right) + \frac{c_0}{2} \frac{\partial^2}{\partial y^2} \left( \int R dr \right) - \frac{1}{2} \tilde{\zeta} \left( \frac{\partial^2 R}{\partial r^2} + \frac{1}{r} \frac{\partial R}{\partial r} \right) = 0 \quad (3.21)$$

with:

$$\tilde{\zeta} = \frac{\left[ \eta + \frac{4}{3} \mu + \kappa \left( \frac{1}{C_v} - \frac{1}{C_p} \right) \right]}{\rho_0} \quad (3.22)$$

where:

- $\eta$  is the Bulk viscosity.
- $\mu$  is the shear viscosity.
- $\kappa$  is the medium thermal conductivity.
- $C_v$  is the specific heat of air at constant volume.
- $C_p$  is the specific heat of air at constant pressure.

One more time, one can notice than the formulation of the above equation 3.21 is similar to the original NPE 3.18 (as well as the NPE in cylindrical coordinates 3.19); the operator  $\frac{1}{2} \tilde{\zeta} \left( \frac{\partial^2 R}{\partial r^2} + \frac{1}{r} \frac{\partial R}{\partial r} \right)$  has been added to include thermoviscous effects.

### 3.3. Implementation of the NPE

Equation 3.21 is the best candidate for implementation: the model established is able to recreate weakly nonlinear effects, simulate absorption from air, allow the use of spatially-varying quantities (sound celerity, medium density) and solve complex configurations in a reasonable amount of time. The ground is assumed flat and rigid; the problem of impedant ground and complex topography is not addressed in this study. The implementation of equation 3.21 is described in the following section. The equation to be implemented is written below for simplicity:

$$\frac{\partial R}{\partial t} + \frac{c_0}{2} \frac{R}{r} + \frac{\partial}{\partial r} \left( c_1 R + c_0 \frac{\beta}{2} R^2 \right) + \frac{c_0}{2} \frac{\partial^2}{\partial y^2} \left( \int R dr \right) - \frac{1}{2} \xi \left( \frac{\partial^2 R}{\partial r^2} + \frac{1}{r} \frac{\partial R}{\partial r} \right) = 0$$

This equation features:

- cylindrical decay.
- small-angle approximation.
- thermoviscous absorption.
- nonlinearities taken to the first order.

The high-angle approximation presented in section 3.2.3 has not been retained for the implementation. Considering usual distances in this type of calculations (several kilometers), a higher accuracy close to the source is a weak improvement compared to the numerical effort needed to integrate the additional terms. Equation 3.21 is implemented using an operator splitting method. The resulting differential operators are integrated with a Crank-Nicolson (see appendix A) and first order finite differences schemes, except the operator calculating nonlinear effects, which receives a special treatment. It is handled with a flux corrected transport (FCT) algorithm that allows to accurately model shock formation. The boundary conditions on the moving window are then discussed and finally some notes and recommendations on numerical issues that may arise are given.

#### 3.3.1. Operator splitting

An operator splitting method is used to solve the differential equation 3.21. The acoustic pressure field at time  $n + 1$  is calculated in four successive steps:

$$\begin{aligned} R_{i,j}^{n+\frac{1}{4}} &= \Gamma_1 R_{i,j}^n \\ R_{i,j}^{n+\frac{1}{2}} &= \Gamma_2 R_{i,j}^{n+\frac{1}{4}} \\ R_{i,j}^{n+\frac{3}{4}} &= \Gamma_3 R_{i,j}^{n+\frac{1}{2}} \\ R_{i,j}^{n+1} &= \Gamma_4 R_{i,j}^{n+\frac{3}{4}} \end{aligned} \quad (3.23)$$

where  $R_{i,j}^n$  is the numerical solution at location and time  $(x_i, y_j; t_n)$ . The numerical implementation of the different operators is detailed in the following sections:

- $\Gamma_1 = -\frac{c_0}{2} \frac{\partial}{\partial r} \left( c_1 R + \frac{\beta c_0}{2} R^2 \right)$ : nonlinear effects and refraction: section 3.3.2.
- $\Gamma_2 = -\frac{c_0 R}{2r}$ : cylindrical decay: section 3.3.3.
- $\Gamma_3 = \frac{1}{2} \zeta \left( \frac{\partial^2 R}{\partial r^2} + \frac{1}{r} \frac{\partial R}{\partial r} \right)$ : thermoviscous effects: section 3.3.4.
- $\Gamma_4 = -\frac{c_0}{2} \int_{r_f}^r \frac{\partial^2 R}{\partial y^2} dr$ : diffraction: section 3.3.5.

### 3.3.2. Nonlinear effects and refraction

The differential equation to be solved is:

$$\frac{DR}{Dt} = -\frac{\partial}{\partial r} \left( c_1 R + \frac{\beta c_0}{2} R^2 \right) \quad (3.24)$$

Equation 3.24 is a hyperbolic differential equation that can't be solved with traditional finite difference schemes. Discontinuities in the solution (during shock formation) are handled with a flux corrected transport (FCT) algorithm. Such methods show high quality shock resolution and allow to simulate shock formation without introducing numerical oscillations (Gibb's oscillations). Fundamental principles of such algorithms are not given here, only main calculation steps are Given. Detailed descriptions can be found in articles by Védý [58], Sjögreen [51] or Boris [10]. The following notations will be used:

$$\begin{aligned} \Delta_+ R_{i,j}^n &= R_{i+1,j}^n - R_{i,j}^n \\ \Delta_- R_{i,j}^n &= R_{i,j}^n - R_{i-1,j}^n \end{aligned} \quad (3.25)$$

The flux function of equation 3.24 is:

$$f \left( R_{i,j}^n \right) = c_1 R_{i,j}^n + \frac{\beta c_0}{2} \left( R_{i,j}^n \right)^2 \quad (3.26)$$

We define:

- The local wave celerity:

$$a_{i+\frac{1}{2},j} = \begin{cases} \frac{f(R_{i+1,j}^n) - f(R_{i,j}^n)}{R_{i+1,j}^n - R_{i,j}^n} & \text{if } R_{i+1,j}^n \neq R_{i,j}^n \\ f' \left( R_{i,j}^n \right) & \text{if } R_{i+1,j}^n = R_{i,j}^n \end{cases}$$

- The numerical flux of a first order total variation diminishing (TVD) scheme:

$$h_{i+\frac{1}{2},j}^n = \begin{cases} f(R_{i+1,j}^n) & \text{if } a_{i+\frac{1}{2},j} < 0 \\ f(R_{i,j}^n) & \text{if } a_{i+\frac{1}{2},j} > 0 \end{cases}$$

- The numerical viscosity of an upwind-scheme:

$$Q_{i+\frac{1}{2},j} = \frac{\delta t}{\delta x} |a_{i+\frac{1}{2},j}|$$

- The numerical viscosity of a Lax-Wendroff scheme:

$$Q_{i+\frac{1}{2},j}^{LW} = \left(\frac{\delta t}{\delta x}\right)^2 a_{i+\frac{1}{2},j}^2$$

The acoustic pressure field is calculated in two successive steps:

$$\begin{aligned} R_{i,j}^* &= R_{i,j}^n - \frac{\delta t}{\delta x} \Delta_- h_{i+\frac{1}{2},j}^n \\ R_{i,j}^{n+1} &= R_{i,j}^* - \left(b_{i+\frac{1}{2},j} - b_{i-\frac{1}{2},j}\right) \end{aligned} \quad (3.27)$$

With:

$$d_{i+\frac{1}{2},j} = \frac{1}{2} \left(Q_{i+\frac{1}{2},j} - Q_{i+\frac{1}{2},j}^{LW}\right)$$

and:

$$b_{i+\frac{1}{2},j} = \begin{cases} 0 & \text{if } \Delta_+ R_{i,j}^* \Delta_- R_{i,j}^* < 0 \text{ or } \Delta_+ R_{i+1,j}^* \Delta_- R_{i+1,j}^* < 0 \\ \text{sign}(\Delta_+ R_{i,j}^*) \left[ \min\left(\frac{1}{2} | \Delta_- R_{i+1,j}^* |, d_{i+\frac{1}{2},j} | \Delta_+ R_{i,j}^* |, \frac{1}{2} | \Delta_+ R_{i+1,j}^* | \right) \right] & \text{otherwise} \end{cases}$$

Another advantage of this algorithm is that it allows to use a high Courant number. Theoretically, the Courant-Friedrich-Lewy condition for this finite difference scheme allows to use a Courant number  $\frac{\delta t}{\delta x} a_{i+\frac{1}{2},j} < 1$ ; in practice, this number will be limited to 0.8 to ensure numerical stability. A shock formation calculated with the FCT algorithm is shown in Figure 3.2. The peak amplitude of the sinusoid is  $\rho c_0^2$ ; the nonlinearity coefficient used is  $\beta = 1.2$ , corresponding to air under normal atmospheric conditions (1013 hPa, 20 °C).

### 3.3.3. Cylindrical decay

The differential equation to be solved is:

$$\frac{DR}{Dt} = -\frac{c_0 R}{2r} \quad (3.28)$$

First order finite differences schemes and Crank-Nicolson method (see appendix A) are used:

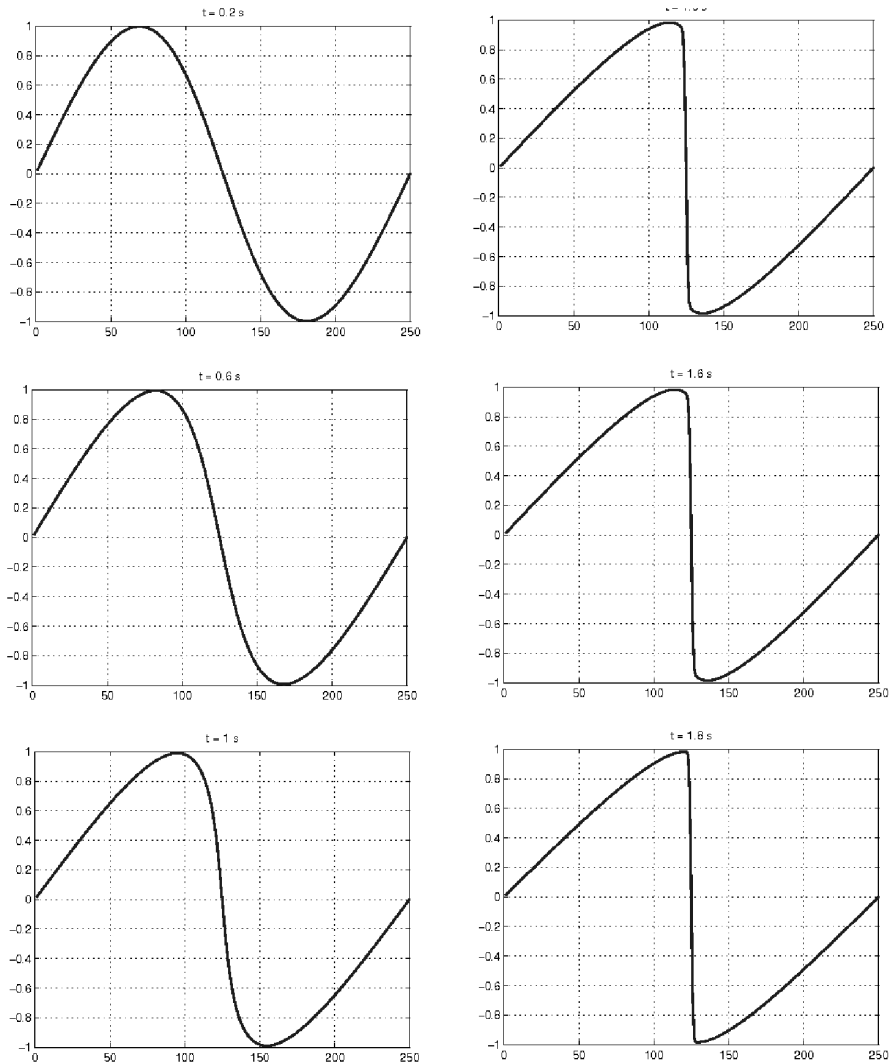


Figure 3.2.: Shock formation from a sinusoid: the initial wave slowly evolve to a N-wave. The amplitude is here normalized to  $\rho c_0^2$ . The nonlinearity coefficient used is  $\beta = 1.2$  (air at 20 °C under 1013 hPa).

$$R_{i,j}^{n+1} - R_{i,j}^n = -\frac{c_0 \delta t}{4r} (R_{i,j}^{n+1} + R_{i,j}^n) \quad (3.29)$$

We define  $\alpha = -\frac{c_0 \delta t}{4r}$ . Gathering together the common terms one can find from equation 3.29:

$$R_{i,j}^{n+1} = \frac{1 + \alpha}{1 - \alpha} R_{i,j}^n \quad (3.30)$$

The new field  $R_{i,j}^{n+1}$  can be calculated by multiplying the previous pressure distribution by a coefficient depending on the distance already traveled. The parameter  $\alpha$  being negative, the wave amplitude is decreasing as it propagates, as expected.

### 3.3.4. Thermoviscous effects

The differential equation to be solved is:

$$\frac{DR}{Dt} = \frac{1}{2} \zeta \left( \frac{\partial^2 R}{\partial r^2} + \frac{1}{r} \frac{\partial R}{\partial r} \right) \quad (3.31)$$

First order finite differences scheme and Crank-Nicolson (see appendix A) method are used:

$$R_{i,j}^{n+1} - R_{i,j}^n = \frac{\delta t \zeta (2r \delta y + \delta y^2)}{8r \delta y^3} (R_{i+1,j}^{n+1} - 2R_{i,j}^{n+1} + R_{i-1,j}^{n+1}) \\ + \frac{\delta t \zeta (2r \delta y + \delta y^2)}{8r \delta y^3} (R_{i+1,j}^n - 2R_{i,j}^n + R_{i-1,j}^n)$$

We define  $\beta = \frac{\delta t \zeta (2r \delta y + \delta y^2)}{8r \delta y^3}$ . Equation 3.32 becomes:

$$R_{i,j}^{n+1} - R_{i,j}^n = -2\beta (R_{i,j}^{n+1} + R_{i,j}^n) + \beta (R_{i+1,j}^{n+1} + R_{i-1,j}^{n+1}) + \beta (R_{i+1,j}^n + R_{i-1,j}^n) \quad (3.32)$$

Gathering together the common terms one can find:

$$R_{i,j}^{n+1} (1 + 2\beta) - \beta (R_{i+1,j}^{n+1} + R_{i-1,j}^{n+1}) = R_{i,j}^n (1 - 2\beta) + \beta (R_{i+1,j}^n + R_{i-1,j}^n) \quad (3.33)$$

Equation 3.33 can be written as a tridiagonal linear equations system which can easily be solved with a Thomas algorithm (see appendix A):

$$\begin{bmatrix} (1 + 2\beta) & -\beta & & \\ & \ddots & \ddots & \\ & & -\beta & (1 + 2\beta) \end{bmatrix} \cdot \begin{Bmatrix} R_{1,j}^{n+1} \\ \vdots \\ R_{N_x,j}^{n+1} \end{Bmatrix} \\ = \\ \begin{bmatrix} (1 - 2\beta) & \beta & & \\ & \ddots & \ddots & \\ & & \beta & (1 - 2\beta) \end{bmatrix} \cdot \begin{Bmatrix} R_{1,j}^n \\ \vdots \\ R_{N_x,j}^n \end{Bmatrix}$$

### 3.3.5. Diffraction

The diffraction operator is:

$$\frac{DR}{Dt} = -\frac{c_0}{2} \int_{r_f}^r \frac{\partial^2 R}{\partial z^2} dr \quad (3.34)$$

where  $r_f$  is a point in the moving window ahead of the wave, where the medium is quiescent. A Crank-Nicolson scheme (see appendix A) for the spatial derivatives and a centered finite difference scheme for the temporal derivative are used. Equation 3.34 can be transformed:

$$\begin{aligned} R_{i,j}^{n+1} - R_{i,j}^n = & -\frac{c_0 \delta t}{4\delta z^2} \int_{r_f}^r \left\{ R_{i,j+1}^{n+1} - 2R_{i,j}^{n+1} + R_{i,j-1}^{n+1} \right\} dr \\ & -\frac{c_0 \delta t}{4\delta z^2} \int_{r_f}^r \left\{ R_{i,j+1}^n - 2R_{i,j}^n + R_{i,j-1}^n \right\} dr \end{aligned} \quad (3.35)$$

A trapezoidal law is used to calculate the integral<sup>2</sup>:

$$\int_{r_f}^r R_{i,j}^n = \delta x \left[ \frac{1}{2} \left( R_{N_x,j}^n + R_{i,j}^n \right) + \sum_{m=N_x-1}^{i+1} R_{m,j}^n \right] \quad (3.36)$$

The fact that  $R_{N_x,j}^n = 0$  (point ahead of the perturbation) is used to eliminate it in the above expression. One can now use the expression of the integral to insert it in equation 3.35:

$$\begin{aligned} R_{i,j}^{n+1} (1 + 2A) - A \left( R_{i,j+1}^{n+1} + R_{i,j-1}^{n+1} \right) = & R_{i,j}^n (1 - 2A) + A \left( R_{i,j+1}^n + R_{i,j-1}^n \right) \\ & + 2A \sum_{m=N_x-1}^{i+1} \left[ R_{m,j+1}^{n+1} - 2R_{m,j}^{n+1} + R_{m,j-1}^{n+1} \right] \\ & + 2A \sum_{m=N_x-1}^{i+1} \left[ R_{m,j+1}^n - 2R_{m,j}^n + R_{m,j-1}^n \right] \end{aligned} \quad (3.37)$$

Where  $A = -\frac{c_0 \delta t \delta x}{8\delta z^2}$ . One more time all terms containing the field at time  $n + 1$  are moved to the right-hand side and the equation is written in a matricial form:

$$\begin{bmatrix} (1 + 2A) & -A & & & \\ & \ddots & \ddots & \ddots & \\ & & -A & (1 + 2A) & -A \\ & & & \ddots & \ddots & \ddots \\ & & & & -A & (1 + 2A) \end{bmatrix} \cdot \begin{Bmatrix} R_{i,1}^{n+1} \\ \vdots \\ R_{i,j}^{n+1} \\ \vdots \\ R_{i,N_z}^{n+1} \end{Bmatrix}$$

<sup>2</sup>The order of the sum limits may seem inversed: the integration is done from right to left, taking the right-most point as initial point.

$$\begin{aligned}
&= \\
&\left[ \begin{array}{ccccccc}
(1-2A) & A & & & & & \\
& \ddots & \ddots & \ddots & & & \\
& & A & (1-2A) & A & & \\
& & & \ddots & \ddots & \ddots & \\
& & & & A & (1-2A) & \\
& & & & & & 
\end{array} \right] \cdot \left\{ \begin{array}{c} R_{i,1}^n \\ \vdots \\ R_{i,j}^n \\ \vdots \\ R_{i,N_z}^n \end{array} \right\} \\
&+ \\
&\left\{ \begin{array}{c} \sum_{m=N_x-1}^{i+1} [R_{m,2}^n - 2R_{m,1}^{n+1} + R_{m,2}^{n+1} - 2R_{m,1}^{n+1}] \\ \vdots \\ \sum_{m=N_x-1}^{i+1} [R_{m,j+1}^n - 2R_{m,j}^{n+1} + R_{m,j-1}^n + R_{m,j+1}^{n+1} - 2R_{m,j}^{n+1} + R_{m,j-1}^{n+1}] \\ \vdots \\ \sum_{m=N_x-1}^{i+1} [-2R_{m,N_z}^n + R_{m,N_z-1}^n - 2R_{m,N_z}^{n+1} + R_{m,N_z-1}^{n+1}] \end{array} \right\}
\end{aligned}$$

One more time the above equation leads to a tridiagonal linear equations system solved with a Thomas algorithm (see appendix A). Numerical integration is made column by column, from the right side of the window to the left side, so that the terms appearing in the sums are known.

### 3.3.6. Boundary conditions

In this section the boundary conditions used in the model are detailed. Three types of boundary conditions are needed to completely bound the calculation grid: the lateral boundaries (right-most and left-most points of the grid), the bottom row of the domain and the absorbing layer at the top of the grid.

#### Lateral conditions

The lateral boundaries of the moving window have no physical meaning. The window represents a domain where the signal can evaluate; it *must not* reach the lateral boundaries, otherwise it will exit the computational domain. One has to be very careful with this restriction and choose a window that is large enough considering the wave celerity *within* the window, so that the signal stays in the computational grid. This condition is ensured by setting the left-most column to 0 and checking at each time iteration that it remains null. In addition, the right-most point has been taken as the initial point in the expression of the integral of the diffraction term so that it can be eliminated (equation 3.36 in section 3.3.5). This force the last column of the grid to be equal to 0.

## Ground

The ground is numerically represented by the first row of the computational grid. Although ground impedance could be used in this finite difference model, only rigid ground conditions are implemented. This choice is made to simplify the model and allow to spend more time on other important topics. This assumption of a rigid ground is not so restrictive: propagated signals have a low frequency content, and at these frequencies the reflection coefficient is close to unity. A rigid boundary condition  $\partial p / \partial n = 0$  is incorporated by assuming a solution which is symmetric with respect to the boundary and modifying the recurrence accordingly for the boundary nodes. Note that this boundary condition only appears in the diffraction operator; the other finite difference schemes don't use pressure value at location  $(i, j - 1)$ . The reformulation of equation 3.37 including the rigid boundary condition gives an expression for the field on the ground layer:

$$R_{i,0}^{n+1} (1 + 2A) - 2AR_{i,1}^{n+1} = R_{i,0}^n (1 - 2A) + 2AR_{i,1}^{n+1} + 4A \left( \sum_{m=N_x-1}^{i+1} [R_{m,1}^{n+1} - R_{m,0}^{n+1}] + \sum_{m=N_x-1}^{i+1} [R_{m,1}^n - R_{m,0}^n] \right) \quad (3.38)$$

## Absorbing layer

Physically, the domain is semi-infinite, i.e. sound waves can propagate beyond the top layer with no restrictions. An absorbing layer has to be implemented to artificially absorb the waves that would exceed the top layer and preventing them from being reflected into the computational domain. A lossy medium is used near the computational edge to attenuate outgoing waves. However, since there is always a reflection between layers with difference absorption coefficients, this boundary condition requires a substantial number of layers with a tapered profile of absorption. The absorption in the layer is incorporated with the help of a new finite difference operator:

$$\frac{DR}{Dt} = -\frac{1}{\tau}R \quad (3.39)$$

Where  $\tau$  is an absorption coefficient chosen according to Abbaléa [2] (Phd thesis in french) and is equal to:

$$\tau = \frac{\delta t}{2} \left( \frac{z - z_{sup}}{z_{max} - z_{sup}} \right)^2 \quad (3.40)$$

Where  $z_{max}$  is the maximum altitude of the domain (including the absorptive layer) and  $z_{sup}$  is the maximum altitude of the physical domain. This operator is implemented in a similar way as for the other finite difference operator: a Crank-Nicolson and centered

finite difference schemes are used. We end with the following equation:

$$R_{i,j}^{n+1} = - \left( \frac{1 - \frac{\delta t}{2\tau}}{1 + \frac{\delta t}{2\tau}} \right) R_{i,j}^n \quad (3.41)$$

One can note that the application of the operator 3.39 results in the multiplication of the field by an absorption coefficient:

$$A = - \frac{1 - \frac{\delta t}{2\tau}}{1 + \frac{\delta t}{2\tau}} \quad (3.42)$$

Figure 3.3 shows this coefficient along with the altitude. The absorption coefficient gradually increases from 0 to 100 %. This slowly-varying absorption is extremely important to prevent reflections between two consecutive layers. During the implementa-

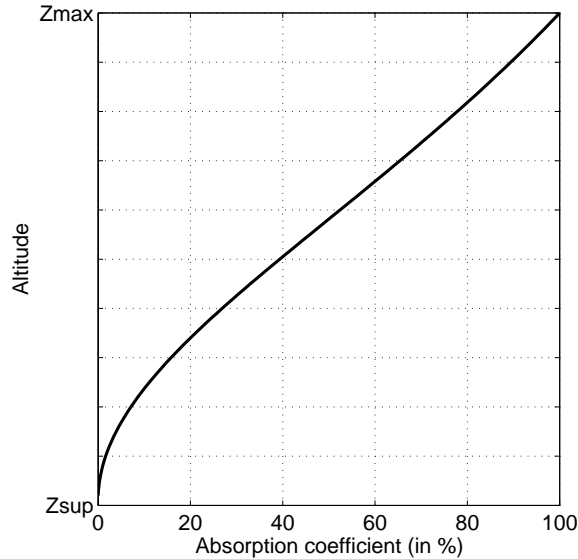


Figure 3.3.: Absorption coefficient in the absorbing layer. The absorption slowly increases from 0 to 1, providing progressive attenuation to prevent reflections.

tion and testing period, a lot of different expressions for this absorption coefficient have been assessed. It appears that the quantity described in equation 3.42 was the most effective; nevertheless, the number of absorption layers has still to be large: typically one fifth to one third of the physical domain, which greatly increase the computational effort. Figure 3.4 shows a schematic diagram representing all the boundary conditions (absorption layer, lateral and ground boundaries) on the moving window.

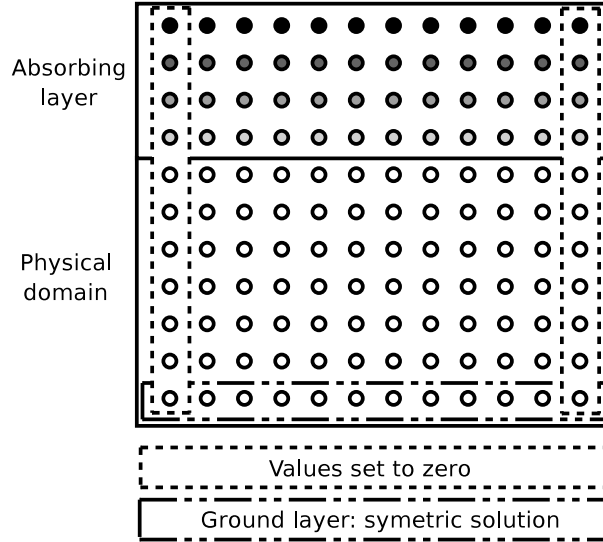


Figure 3.4.: Schematic representation of the computational grid. The values at points on ground layer are calculated by assuming a symmetric solution; the edge columns are set to 0. The absorption area contains several layers with progressive absorption to prevent from reflections of outgoing waves.

### 3.4. Numerical considerations

The semi-implicit time advancement scheme presented for cylindrical decay, thermo-viscous effects and diffraction is stable for all  $\delta t$ . The Courant-Friedrich-Lewy (CFL) stability condition for the nonlinear effects and refraction operator is:

$$\delta t < \frac{\delta x}{a_{i+\frac{1}{2},j}}$$

where  $a_{i+\frac{1}{2},j}$  is the local wave celerity and is defined as:

$$a_{i+\frac{1}{2},j} = \begin{cases} \frac{f(R_{i+1,j}^n) - f(R_{i,j}^n)}{R_{i+1,j}^n - R_{i,j}^n} & \text{si } R_{i+1,j}^n \neq R_{i,j}^n \\ f'(R_{i,j}^n) & \text{si } R_{i+1,j}^n = R_{i,j}^n \end{cases}$$

In practise, the CFL number must be limited to lower values (typically 0.8) to ensure stability. The local wave celerity depends on the signal amplitude, the CFL condition has thus to be checked for every position in the grid. A good choice for the time step  $\delta t$  is to fix it to  $\delta t = \delta x / c_{win}$ . In this way, for each time iteration, the window advances one spatial step. This produces clean time signal (no spatial interpolation needed) and also ensure numerical stability even for very high amplitudes.

The window wave celerity  $c_{win}$  has been chosen so that the sound speed perturbation  $c_1(x, y)$  is negative, and thus, the signal propagates backward in the window. One could think about the opposite solution: defining  $c_{win} = \min(x, y)$  gives a positive sound celerity perturbation and thus a forward propagation in the window. This solution may appear simpler but is not necessarily a good choice. The signal will have to be placed somehow in the middle of the window so that diffraction effects can occur in the left side of the window and that wave propagation, due to sound speed perturbations, can occur in the right side of the window. This solution would require a larger window and thus significantly increases the computational time. In the case of constant sound speed profile, both methods could be used.

Nonlinear effects and refraction, cylindrical decay and thermoviscous effects operators operates only along a single line (the diffraction operator is the only one to use quantities up and down the calculated value). It means that to gain computational time, it is not necessary to apply this operators inside the absorption layer.

Diffraction operator leads to a tridiagonal linear equations system that is solved with a Thomas algorithm. One may consider calculating the left hand side matrix before the iteration loop. Indeed, coefficients appearing in the left hand side terms are constant; calculating these values previously to the iteration loop may save a substantial amount of computational time. If sound diffusivity is chosen constant with altitude the same method can be applied to the thermoviscous effects operator.

One tricky task in the choice of parameters is the determination of the window width through the parameters  $\delta x$  and the number of points. While the spatial discretization step  $\delta x$  can't vary a lot for accuracy reasons, the number of points can adopt a wide range of values depending on the problem configuration. In the case of spatially-varying sound celerity, the number of points has to be sufficient so that the wave can evaluate within the window without reaching the edges of the domain, but the number of points chosen should be kept as low as possible to limit the computational time. For complex configurations, a hand calculation is more than recommended: taking the maximum sound celerity *perturbation* in the window and multiplying with the propagation time wanted gives the maximum distance traveled by the wave *within the window*.

## 4. Model validation

The aim of this chapter is to present the model validation process. Correcting bugs, testing, improving the code and adding functionalities is a very long procedure that preceded the model validation. The full validation of the model has been separated in two tasks: first nonlinear effects are assessed using 1D analytical solutions and then a linear propagation configuration is studied to validate phenomena such as refraction, sound celerity, reflections on the ground or atmospherical absorption. Although many validation cases have been studied, from the simplest to very complex cases, only one simulation that allows to fully validate the numerical method is presented. For this linear propagation configuration the solutions are compared to the results given by the ATMOS (Advanced Theoretical Model for Outdoor Sound propagation) propagation code, an implementation of the parabolic equation previously developed at the CSTB.

### 4.1. Nonlinear effects

#### 4.1.1. Fubini's solution

Fubini developed a solution for the nonlinear propagation of monofrequency sources. The solution is presented in section 2.5.1 and is reminded here for simplicity. The pressure distribution is expressed by an infinite sum of weighted Bessel functions:

$$p(\sigma, \tau) = p_0 \sum_{n=1}^{\infty} \frac{2}{n\sigma} J_n(n\sigma) \sin(n\omega\tau) \quad (4.1)$$

where  $\sigma = x/\bar{x}$ ,  $\tau = t - x/c_0$ ,  $p_0$  is the initial sinusoid amplitude,  $J_n$  is the Bessel function of order  $n$  and  $\bar{x}$  is the shock formation distance. The formulation presented in equation 4.1 gives valid solutions for 1D problems only in the pre-shock region ( $\sigma < 1$ ). In addition, losses are not included in the model.

#### 4.1.2. Results

Results of nonlinear calculations given by the NPE are compared to analytical Fubini's solution. Since the operator calculating nonlinear effects and refraction operates over a single direction the problem is considered one-dimensional. The wave celerity used is  $c = 343$  m/s and the nonlinearity coefficient is  $\beta = 1.2$  (air at 20 °C under 1 atm). The

peak amplitude of the wave is 10 kPa (174 dB re 20  $\mu$ Pa) and its frequency is 0.1 Hz. The wave deformation can be observed on Figure 4.1, which presents the original sine wave together with two snapshots at time 6.4 and 12.8 seconds. The criteria to evaluate the performances of the NPE is the harmonics amplitudes evolution. During the sine-wave deformation, the amplitude of the fundamental frequency decreases, and the amplitude of higher harmonics increases. Figure 4.2 presents the evolution of the fundamental frequency, first and second harmonics amplitudes over time. The simulation ran for 120 time steps and has been stopped just before the shock formation, where the Fubini's solution is no longer valid.

The results given by the implemented NPE are close to the analytical solution. The maximum relative error is 0.4% for the fundamental frequency amplitude. For the first and second harmonics the maximum relative errors are 2 % and 3.5 %, respectively, provided their values are much greater than numerical uncertainty. Indeed, one may note that the relative difference between the models may be very high (for example: third harmonic amplitude, at the beginning of the simulation). This is due to the fact that the amplitude is extremely low at this stage of the simulation. As a result relative errors are large, but as the simulation goes on it quickly decreases. Nonlinear effects are accurately simulated by the implemented NPE.

## 4.2. Complex linear case

### 4.2.1. ATMOS sound propagation code

ATMOS stands for Advanced Theoretical Model for Outdoor Sound propagation. Designed and developed by CSTB researchers, ATMOS is a software which determines the acoustic impact of all types of infrastructures, both near and far away, on their environment, taking the geometry of the site into account as well as the meteorological factors inherent to each local climate. Furthermore, ATMOS is also being used as a "reference numerical model" within the European Harmonoise and Imagine projects dedicated to developing a harmonised method for predicting outdoor noise, in accordance with European Directive 2002/49/EC of 25 June 2002, relating to the assessment and management of environmental noise. It implements a parabolic equation, a frequency domain method that allows to simulate long-rangesound propagation. This code is used in this study as a validation tool for linear propagation problems. Transmission losses from both calculations will be compared to assess the accuracy of the implemented nonlinear progressive wave equation. The transmission loss is defined as the ratio in decibels between the acoustic intensity  $I(x, y)$  at a field point and the intensity  $I_0$  at 1 m distance

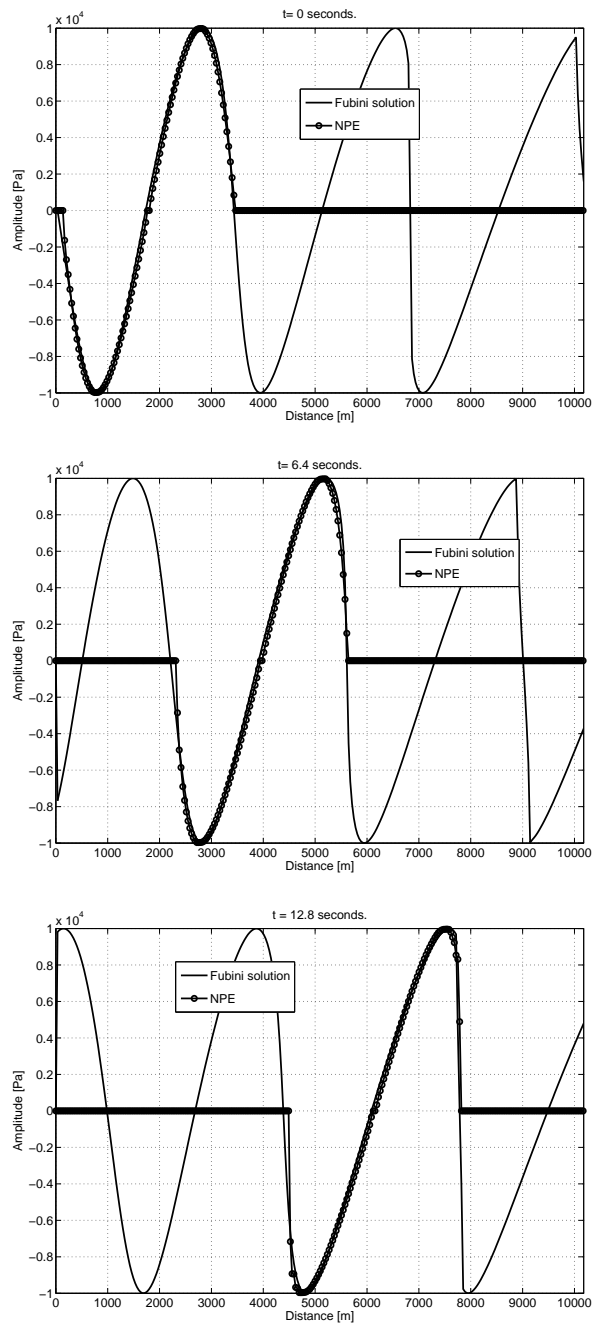


Figure 4.1.: Deformation of a sine wave calculated with the Fubini's solution and the NPE. The three plots show the wave at time: 0, 6.4 and 12.8 seconds.

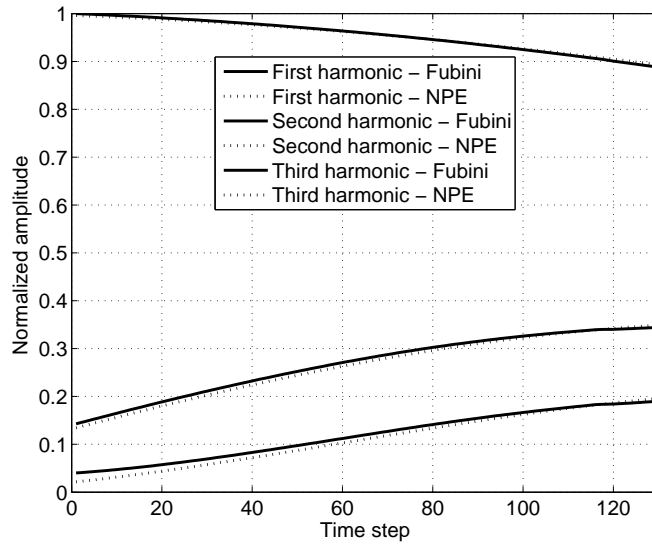


Figure 4.2.: Fundamental and harmonics amplitudes evolution. The curves present solutions given by Fubini and NPE calculations. From top to bottom: fundamental amplitude, first and second harmonics amplitudes, respectively.

from the source, *i.e.*,

$$\begin{aligned}
 TL &= -10 \log \frac{I(x, y)}{I_0} \\
 &= -20 \log \frac{|p(x, y)|}{p_0} \text{ [dB re 1m]}.
 \end{aligned} \tag{4.2}$$

#### 4.2.2. Coupling with ATMOS

In order to use this propagation code as a comparison tool, the sources used in the NPE calculations, that are spatial pressure distributions, have to be transformed into frequency domain “starter” that serve as an input in the ATMOS software. The pressure signal is recorded along a vertical line and transformed into frequency domain with the help of a Fourier transform. This coupling method has been validated with a simple configuration: the (linear) propagation of a monofrequency wave is studied both with the NPE and ATMOS. The sound celerity is constant with altitude and the source is placed on the ground. The coupling between the models has been done at two different distances: 46 km and 112 km. Figure 4.3 shows the transmission loss at 2 m high, calculated with ATMOS, NPE+ATMOS (coupling at 46 km) and NPE+ATMOS (coupling at 112 km). All the calculations lead to the same results. Note that the curves calculated with the coupling method take some time to converge to the exact solution.

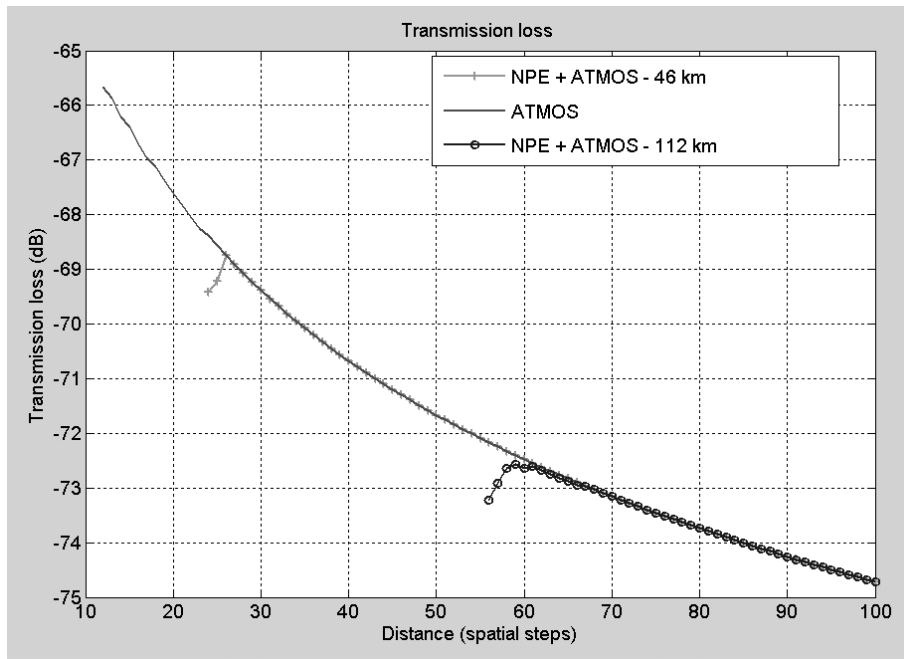


Figure 4.3.: Transmission loss calculated with single ATMOS calculations, and two coupled simulations. Spatial steps are used instead of distance for simplicity.

With this method, one could think of using the NPE to handle nonlinear effects and then use the coupling method and finish the calculations with ATMOS (see schematic in Figure 4.4). The advantage is that ATMOS can handle more complex configurations (non-rigid and non-flat ground) and that it is faster *for monofrequency calculation*. Indeed the parabolic equation is a very fast method, but for broad-band signals, the calculation has to be repeated for each frequency line and this may result in an extremely long calculation for high-resolution spectra. Many cases were tested and it appeared that unless a specific and reduced frequency range is of interest, it is much faster to use the time domain NPE.

Now arise the question: *When should we initialize the coupling ?*. The most convenient (and most used) criteria is the maximum amplitude of the signal. The limit under which one can consider that nonlinear effects are weak is 100 Pa (134 dB re 20  $\mu$ Pa). This limit is taken from the literature and comes from simulations and experiments, it has no physical foundations. The choice of the parameter and its value are discussed in the next chapter: Case Study, where an explosion signal propagation is simulated.

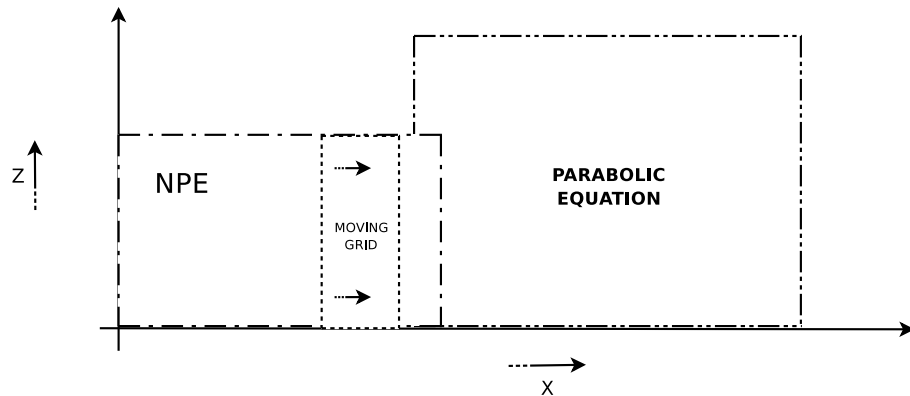


Figure 4.4.: Schematic of the coupling method between the NPE and ATMOS.

### 4.2.3. Results

The propagation of a low frequency wave is studied. The calculation window is 2001 points large in both directions and the absorption layer is 1000 points high (one third of the computational domain). The spatial discretization steps have both been chosen equal to 1 m. With a minimum resolution of  $10 \text{ pt}/\lambda$ , these spatial steps allow to model waves containing frequencies up to 34.3 Hz (with  $c = 343 \text{ m/s}$ ). The simulation ran for 30 000 iterations which resulted in the calculation over a domain which is 2 km high and 30 km wide. The time step is chosen according to the recommendations explained in section 3.4 and is equal to 2.7 ms. The source is a gaussian spatial distribution, which central frequency is 10 Hz and peak amplitude is 1 kPa (154 dB re 20  $\mu\text{Pa}$ ); it is set at altitude  $y = 400 \text{ m}$  close to the right edge of the computational domain (the signal propagates backward in the window). The sound speed profile chosen is shown in Figure 4.5 (the wave speed only varies with the altitude). Although this profile may not be extremely realistic it has the advantage of presenting a lot of variations and thus allows to fully estimate the accuracy of refraction effects calculations. The window is moving with the maximum wave speed which is 363.2 m/s and the maximum wave celerity perturbation is  $c_{1,\text{max}} = 22.2 \text{ m/s}$  and occurs at a 1550 m altitude. The medium properties at rest are those found for a temperature of 20 °C under 1 atm (the nonlinearity coefficient  $\beta$  is here set to zero, since we only consider linear propagation).

The pressure field over the calculation grid was recorded during the iteration process; some of these recordings are shown on Figure 4.6. These six snapshots were taken every 6.85 s starting from time 1.37 s (time evolution in the subplots is from left to right and top to bottom). The white dot in the first subplot represents the position of the source. One can see the spherical wavefront in the first plot, then the reflection on the ground (second plot) and the gradual deformation into a complex shape, due to refraction effects on the following subplots.

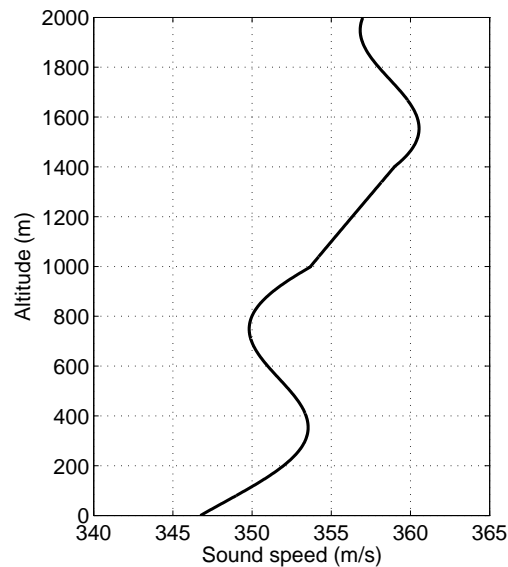


Figure 4.5.: Sound speed profile used in the linear complex case.

Although these movie snapshots can help understand the refraction phenomena, they can hardly be used for quantitative assessment. Transmission loss is calculated with the NPE and ATMOS. The map obtained from the NPE calculations is presented in Figure 4.7. Again one can clearly see on this Figure the effects of spatially-varying meteorological conditions. The globally increasing sound speed produces a downward refraction. The transmission loss is also calculated with ATMOS and the relative difference between models is shown on Figure 4.8. White areas denote a relative difference lower than 2 dB. Transmission loss at three different altitudes (0.5, 1 and 1.5 km) for both linear simulations are also shown on Figure 4.9. On most of the domain the difference between the models is acceptable. A zone near the source presents higher differences: around 3~4 dB. This zone of lower accuracy is due to the coupling method: as shown in section 4.2 the solution from coupled NPE-ATMOS models take some time to converge to the exact solution. Some small and localized areas also present variations higher than 2 dB but the relative difference never exceeds 4 dB.

### 4.3. Conclusion

The implemented NPE has been proven to accurately recreate nonlinear effects, such as wave steepening or dissipation at the shock. This test-case has been done for a one-dimensional problem, but the one-way propagation hypothesis of the nonlinear progressive wave equation ensures the validity of nonlinearity calculations for two-

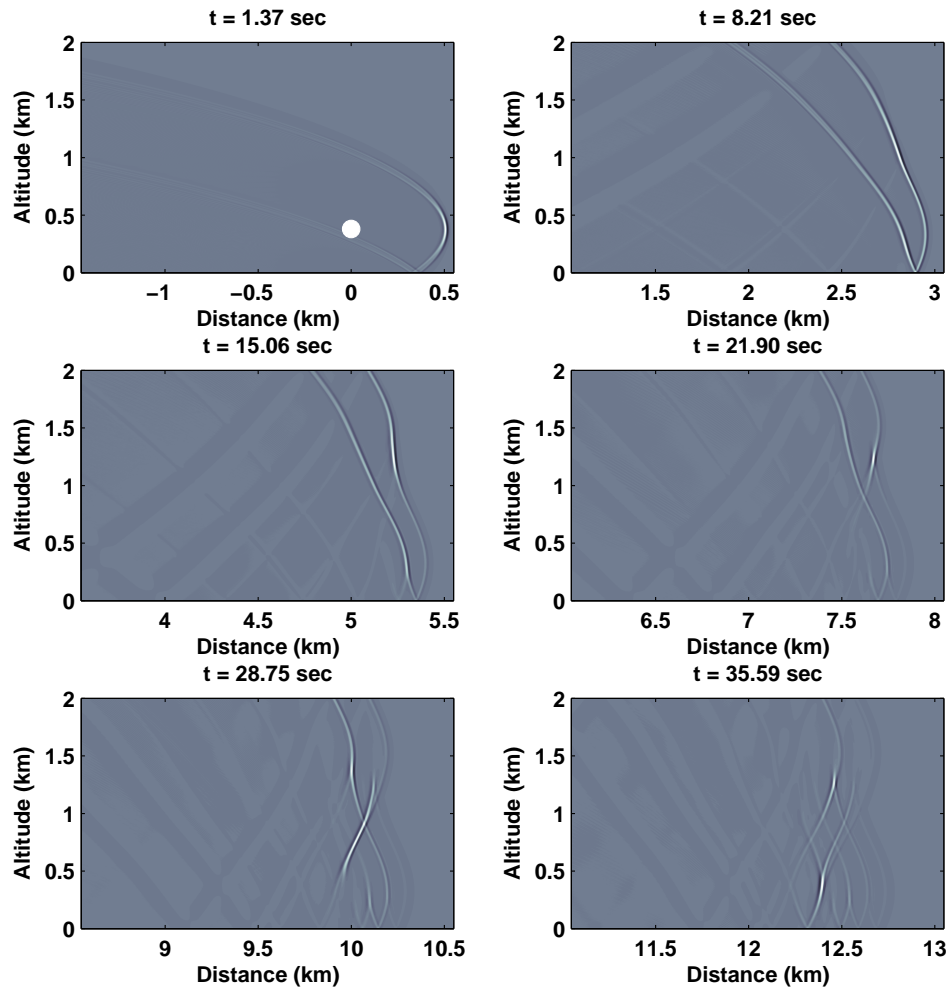


Figure 4.6.: Wave front evolution. These six snapshots were taken every 6.85 s starting from time 1.37 s. Time evolution in the subplots is from left to right and top to bottom. The white dot in the first subplot represents the position of the source.

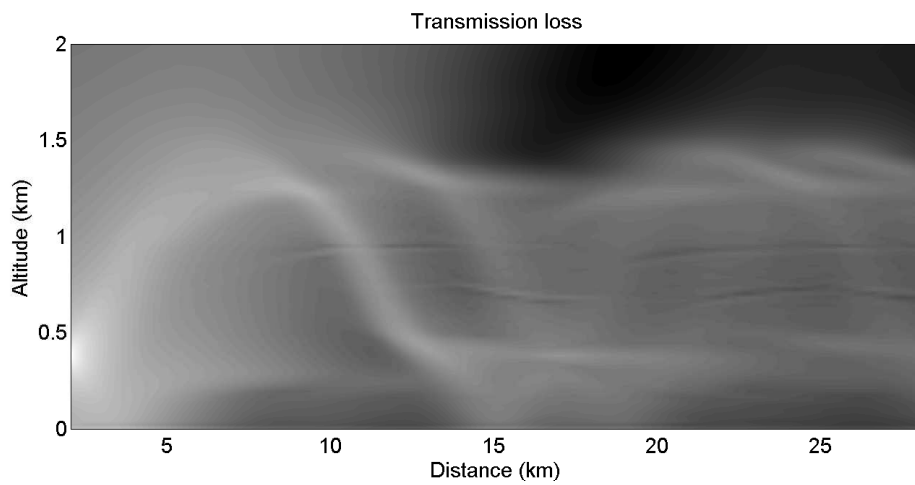


Figure 4.7.: Transmission loss vertical maps obtained with the NPE calculations.

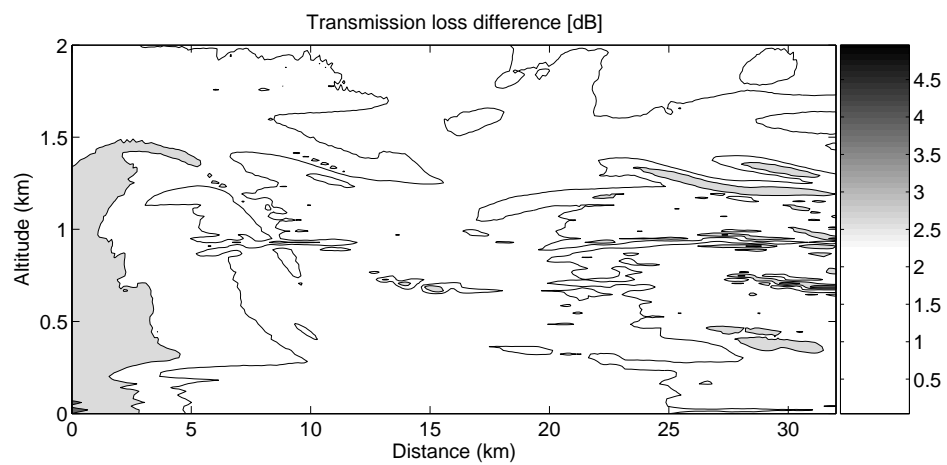


Figure 4.8.: Transmission loss relative difference between ATMOS and NPE calculations. White areas are below 2 dB.

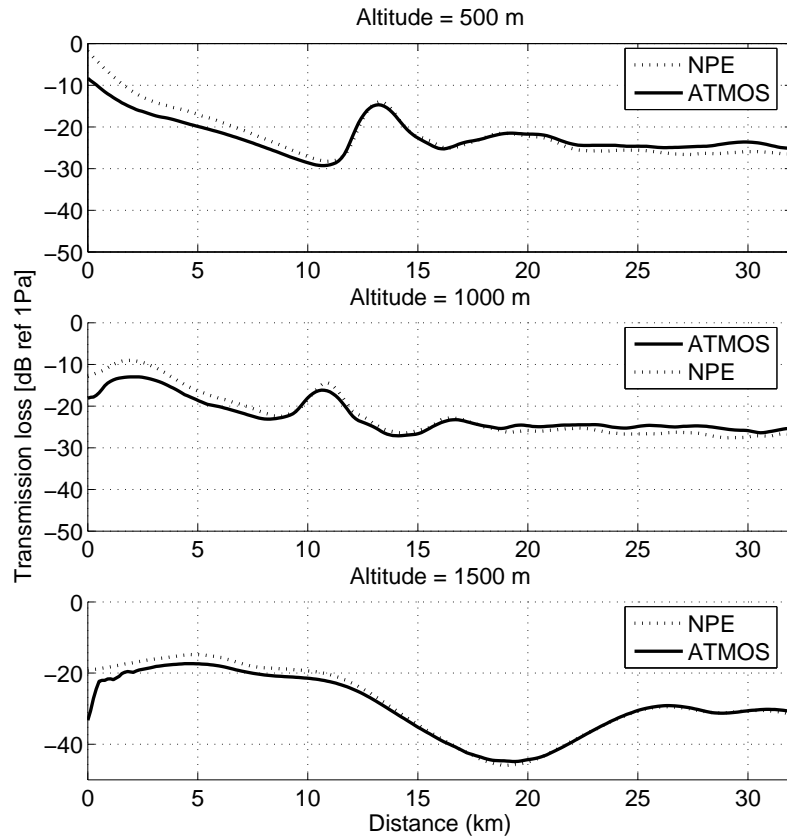


Figure 4.9.: Transmission loss at three different altitudes (0.5, 1 and 1.5 km) for ATMOS and NPE simulations.

dimensional configurations. The numerical method has also been tested regarding meteorological conditions. It appeared that refraction, atmospherical absorption, reflections and interferences were reproduced within a 2 dB relative error range. Of course a full validation problem, including nonlinear effects *and* complex meteorological conditions would have been of great interest. But the lack of data in the litterature and the problems inherent to explosion measurements make it impossible to realize.

The coupling between two different numerical methods has been shown to be successfull. Although algorithms used are very different (time domain/frequency domain), the different methods can be made compatible. Coupling between NPE and, for example, BEM or FEM could be done to study sound barriers or dynamic response of buildings.

## 5. Case study

In this chapter the nonlinear progressive wave equation implemented is used to model the propagation of an explosion born sound wave. The 21<sup>st</sup> of September 2001 a warehouse belonging to the AZF chemical factory in Toulouse (south-west of France) exploded. This accident resulted in many deaths or injured and caused huge damages to buildings in a wide area. The explosion strenght was equivalent to 30 000 tons of TNT. Such powerful detonation produced an acoustic wave of very high amplitude which impact on buildings has been studied at the CSTB in September 2002. Time waveforms were determined with analytical models for explosions (the Kinney-Graham [34] model, see section 5.1). The same model is used at short distances to initialize the calculation window and then the NPE is used to get time waveforms at long ranges. This study focuses on nonlinearities, and their potential effects on structures, due to the high amplitudes of the wave. In section 5.3 the coupling with ATMOS (or any other numerical model) is detailed. Several criteria that could be used to initialize the coupling are compared, and a method to efficiently determine the parameter value is explained. The last section presents a very simple prediction model that allows to know when nonlinearities can be neglected *prior* to the numerical simulation. This analytical model is restricted to a specific class of signals, but it showed to give good results.

### 5.1. Configuration

#### Geometry and meteorological conditions

The nonlinear propagation of the explosion signal is simulated over a domain which is 45 km wide and 1.5 km high. Spatial steps are set to 1.55 meters along the x-axis and 3.10 meters along the vertical axis. The time step is  $\delta t = 4.5$  ms and the simulation ran for 30000 iterations.

The sound speed has been chosen constant over altitude, so that this case study is focused on nonlinear effects. Since the wave will not move within the computational window (constant sound celerity), the grid has been chosen just wide enough to contain the source signal. The window is 120 points large and 500 points high. Chosing a small window reduces the computational time: this simulation ran for 14 minutes on a "normal" desktop computer. A fully linear calculation has also been run to evaluate nonlinearities.

Four receivers are placed in the domain: they are positioned 2 meters high and at 500 m, 1 km, 5 km and 10 km from the source. The source is on the ground and is spherically radiating.

### Source signal

The source signal is determined according to the Kinney-Graham [34] model. This model defines waveforms from chemical and nuclear explosions for an explosion equivalent to 1 kg of TNT:

$$p(t) = p_0 (1 - t/t_d) e^{\alpha t/t_d} \quad (5.1)$$

where  $p(t)$  is the overpressure at time  $t$ ,  $p_0$  is the peak overpressure at time  $t = 0$  ( $t = 0$  at the shock arrival time) and  $t_d$  is the positive phase duration. For a chemical explosion, the ratio of the overpressure to the ambient pressure can be calculated with:

$$\frac{p_0}{p_a} = \frac{808 \left[ 1 + \left( \frac{Z}{4.5} \right)^2 \right]}{\sqrt{1 + \left( \frac{Z}{0.048} \right)^2} \sqrt{1 + \left( \frac{Z}{0.32} \right)^2} \sqrt{1 + \left( \frac{Z}{1.35} \right)^2}} \quad (5.2)$$

where  $Z$  is a reduced distance which units is  $[m/kg^{1/3}]$ . The positive phase duration  $t_d$  is calculated with (again, for a chemical explosion):

$$\frac{t_d}{W} = \frac{980 \left[ 1 + \left( \frac{Z}{0.54} \right)^{10} \right]}{\left[ 1 + \left( \frac{Z}{0.02} \right)^3 \right] \left[ 1 + \left( \frac{Z}{0.74} \right)^6 \right] \sqrt{1 + \left( \frac{Z}{16.9} \right)^2}} \quad (5.3)$$

where  $W$  is a reduced mass. The arrival time  $t_a$  ( $t=0$  in equation 5.1) is calculated with:

$$t_a = \frac{1}{c_0} \int_{r_c}^r \left[ \frac{1}{1 + \frac{6p_0}{7p_a}} \right] dr \quad (5.4)$$

where  $r_c$  is the charge radius and  $r$  is the distance from the source. With this set of equations, time waveforms (and thus spatial waveforms) can be calculated. The TNT equivalent for the AZF explosion has previously been determined to be 30 kT. This value is used in the model; it is assumed that the Kinney-Graham formulas are valid for such explosion strenght. Figure 5.1 presents the source signal used for the calculation and Table 5.1 summarizes the signal characteristics.

## 5.2. Results

Figure 5.2 presents the signals at the receivers for linear (dashed line) and nonlinear (thick line) calculations and Table 5.2 summarizes the evolutions of the properties at the last receiver position (10 km away from the source).

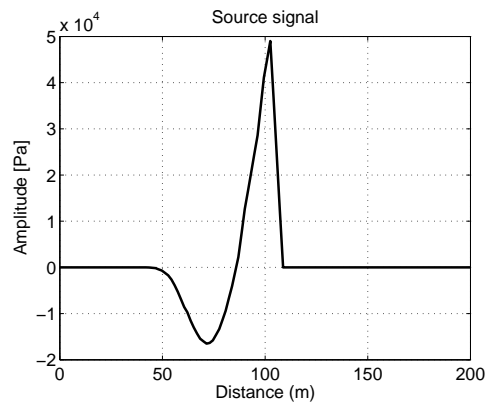


Figure 5.1.: Source signal used in the simulation, calculated with the Kinney-Graham model, for an explosion of 30 kT of TNT.

Positive peak amplitude [kPa]	49
Negative peak amplitude [kPa]	1.65
Positive phase duration [ms]	67.9
Negative phase duration [ms]	108.7
Total duration [ms]	176.6

Table 5.1.: Signal characteristics.

	Linear	Nonlinear	Difference
Arrival time [s]	29.19	29.11	-0.08
Signal duration [ms]	170	270	+100 ms / +58 %
Positive peak amplitude [Pa]	453.4	215.8	-237.6 Pa / -52 %
Positive amplitude duration [ms]	70	150	+80 ms / +53 %
Negative peak amplitude [Pa]	152.4	146.3	-6.1 Pa / -4 %
Negative amplitude duration [ms]	100	120	+20 ms / +20 %
Energy [kPa <sup>2</sup> .s]	5.61	3.17	-2.44 / -43 %

Table 5.2.: Signal properties at 10 km distance; comparison of nonlinear and linear calculations.

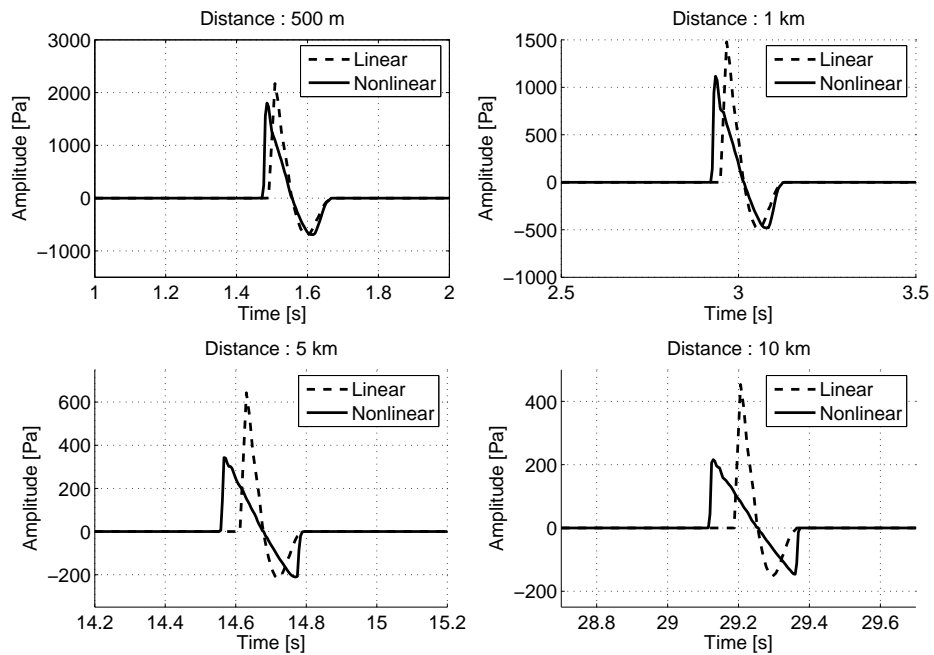


Figure 5.2.: Time signals at the receivers.

Nonlinear effects are clearly visible on all time signals. As expected, the signal from nonlinear calculations travels faster than for linear calculations; the arrival time difference is 80 ms. This value is not crucial for long-rangesound propagation, but it may have its importance in other situations (e.g. room acoustics). One can see on Figure 5.2 that the waveform slowly evolve to an N-wave (or shock wave). The process is gradual and accumulative: effects are still visible even if the signal amplitude is much lower (less than 400 Pa, see two last subplots in Figure 5.2). The positive peak amplitude is greatly reduced (-43 %) by the shock dissipation process; it is less visible (only -6 %) for the negative peak amplitude, since the shock formation occurs later (see two last subplots) and at this time, the wave amplitude approaches nonlinear/linear limit (less than 200 Pa). Another effect of shock formation and dissipation is the modification of signal duration: the signal length is increased (+100 ms / +58%); again, this change is mainly due to the positive amplitude peak. Both peak amplitudes are reduced (in absolute values) but the duration increase is not large enough to compensate for energy losses: it is reduced by 43 %.

Figure 5.3 shows the Fourier transform of signals presented in Figure 5.2. The fundamental frequency shifts from 5 Hz to 2.70 Hz (-46 %) because of the increase of signal duration. This could be of importance regarding building response to explosion noise. First resonance modes of heavy structure are typically below 10 Hz. The fact that

the fundamental frequency decreases with time could lead to high excitation of heavy construction. It could also be noted that the high frequency content changes through propagation: high frequency harmonics are generated.

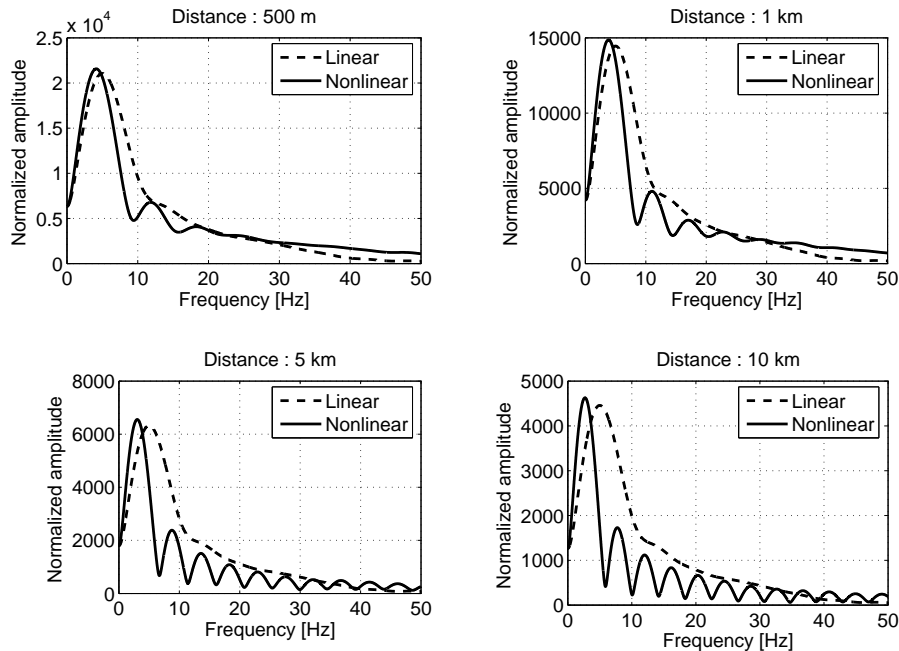


Figure 5.3.: Frequency content of time signals presented in Figure 5.2.

### 5.3. Coupling

Coupling the results of the NPE can be of interest: faster linear propagation code or BEM method could be used to evaluate, for example, the efficiency of protection screens. These methods being linear, the nonlinear effects have to be weak so that output from the NPE can be used as an input for another method. In this section the choice of the parameter (and its value) for an efficient coupling with a linear numerical method is studied. Three parameters are selected:

- The ratio of positive amplitude (nonlinear/linear).
- The ratio of signal durations (linear/nonlinear).
- The ratio of fundamental frequencies (nonlinear/linear).

Figure 5.4 presents the evolution of these parameters through time. All curves follow the same tendency: equal to 1 a time  $t = 0$ , they slowly decrease to their asymptotic

values, as nonlinear effects become less important. The derivatives with respect to time are shown on Figure 5.5: all are very similar. From this observation the hypothesis that the coupling parameter can be chosen arbitrarily can be made. The positive peak amplitude is chosen as a coupling parameter: it is simple and fast to implement (no FFT needed). The curves presented in Figure 5.4 and their derivatives (Figure 5.5) can be modeled by simple equations:

$$f(t) = E + Ae^{(-t/\tau)} \quad (5.5)$$

$$f'(t) = -\frac{A}{\tau}e^{(-t/\tau)} \quad (5.6)$$

where  $E$  is the final ratio (asymptotic value),  $A$  is the variation amplitude and  $\tau$  is a time constant. The analogy with RLC circuits is straightforward: the constant  $\tau$  represents

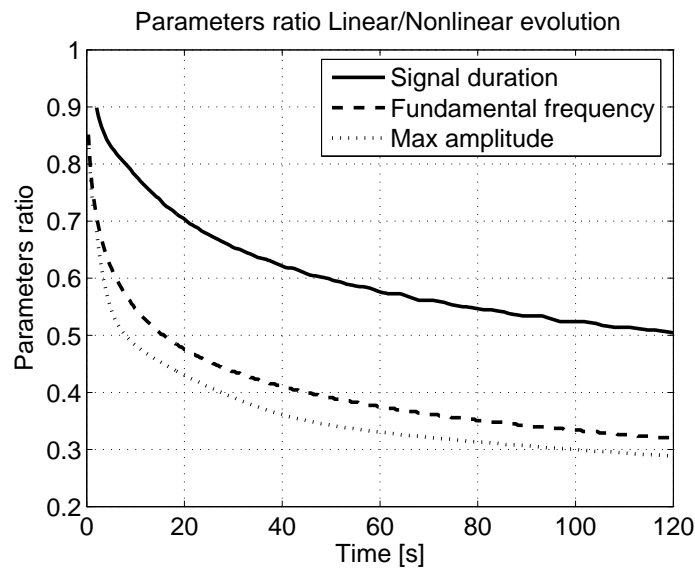


Figure 5.4.: Selected coupling parameters evolution through time.

the time where 63 % of nonlinear effects have already been taken into account. The value of  $\tau$  can geometrically be determined: it is the value where the tangent at  $t = 0$  crosses the x-axis. The value of 63 % is too low to accomplish an efficient coupling; the time where 90 % of nonlinear effects have already been taken into account is chosen instead. Depending on the curve chosen we find the values for  $t_{90}$ :

- Ratio of positive amplitudes (nonlinear/linear):  $t_{90} = 51.5$  s.
- Ratio of signal durations (linear/nonlinear):  $t_{90} = 56.2$  s.
- Ratio of fundamental frequencies (nonlinear/linear):  $t_{90} = 54$  s.

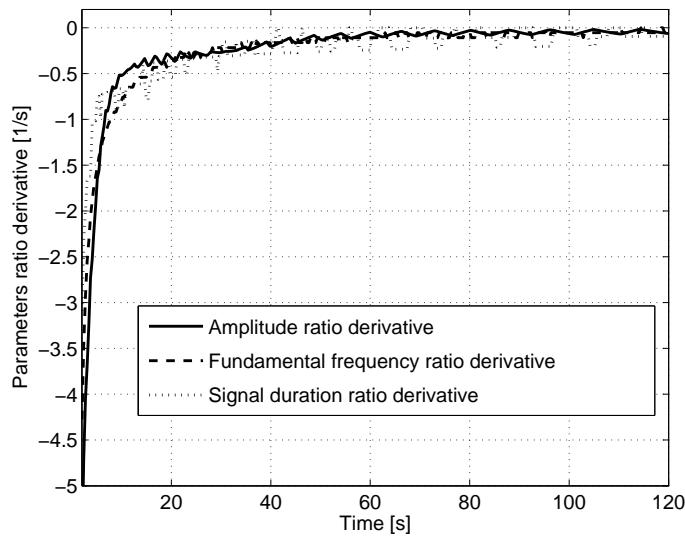


Figure 5.5.: Coupling parameters derivatives evolution through time.

These values are similar and are in accordance with the assumption that the coupling parameter can be chosen arbitrarily. A mean value of  $t_{90} = 54$  s is chosen; at this time, the positive peak amplitude of the signal is  $p_{peak} = 145.5$  Pa. This value is consistent with what is found in the literature: the limiting value where nonlinear effects can be neglected is usually 100 Pa.

To assess the selected parameter value, a fully linear, fully nonlinear and four other coupling values are tested with the configuration presented in section 5.1. The transmission loss is calculated and compared for these seven cases. The selected coupling parameter is the positive peak amplitude and its used values are 500 Pa, 250 Pa, 175 Pa, 145.5 Pa (the value determined above) and 100 Pa. The results are presented in Figure 5.6; the extreme cases, fully linear and fully nonlinear calculations are represented by circle and square lines, respectively. As the coupling value decreases, the curves reach the exact solution, the fully nonlinear line. One can see that the value of 145.5 Pa, previously determined with the help of curves in Figure 5.4 and 5.5, gives very good results. While the coupling value of 175 Pa is (relatively) far from the exact solution, the selected value, only 30 Pa below, is undistinguishable from the exact solution. One should also note that the coupling value of 100 Pa does not give much additional accuracy.

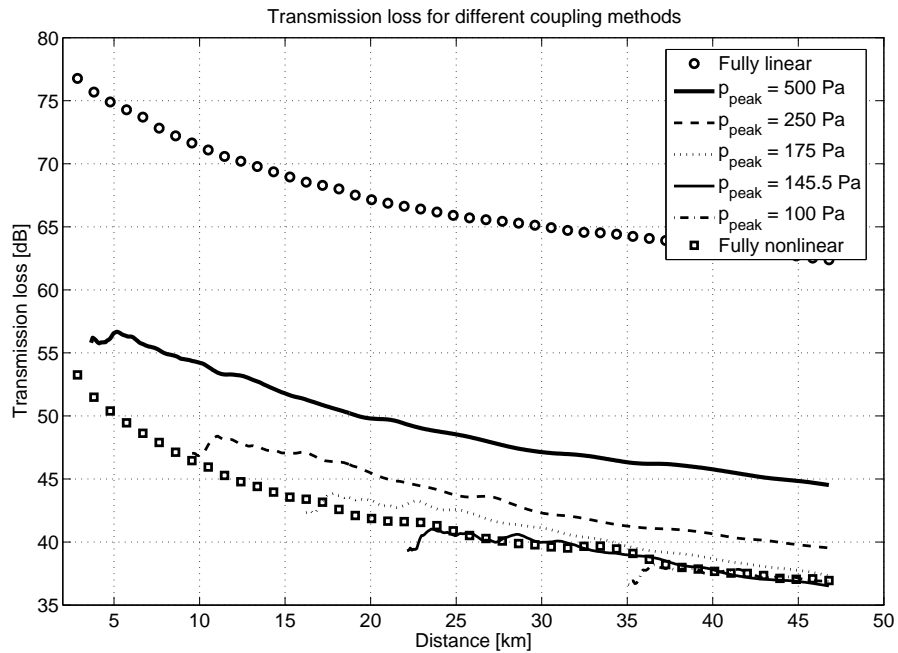


Figure 5.6.: Transmission loss calculated for fully linear, fully nonlinear, and 5 coupling values configurations.

## 5.4. Prediction model

The determination of the coupling parameter value explained above appeared to give excellent results. But the interest stays limited if we're unable to predict the value of the coupling parameter *prior* to the numerical simulation. One could establish an empirical model: testing a lot of different source signals with different characteristics would lead to empirical rules that could be used to predict when nonlinear effects can be neglected. This solution would take a lot of time; another option is to create a simple analytical model for a specific class of signals.

### 5.4.1. Derivation

The aim of this model is to allow someone to know when nonlinear effects can be neglected, with the help of few information on the source signal. The selected criteria is the time  $t_{90}$ , where 90 % of nonlinearities have already been taken into account. For the model to work, source signals must follow some simple rules: the signal must contain *only* one maximum, one minimum and it must cross the x-axis in only one position. These rules are not so restrictive: explosion signals often respect these hypothesis. The

model is based on signal duration increase: it is assumed that before shock formation the signal length remains unchanged and that the shock from positive peak amplitude occurs before the shock from negative peak amplitude. The following notations will be used:

- $A_+(t)$  and  $A_-(t)$  : positive and negative peak amplitudes.
- $d_+(t)$  and  $d_-(t)$  : distance from positive (negative) peak amplitude to the right (left) end of the source signal.
- $L_+(t)$  and  $L_-(t)$  : positive (negative) phase distance.
- $\tau_+$  and  $\tau_-$  : positive and negative shock formation time.
- $\Delta c_+(t)$  and  $\Delta c_-(t)$  : wave celerity increase (decrease) at positive (negative) peak amplitude.
- $\Delta L(t)$  : signal length increase.

Only six parameters describing the source signal are needed for the calculation:  $A_+(0)$  and  $A_-(0)$ ,  $d_+(0)$  and  $d_-(0)$  and  $L_+(0)$  and  $L_-(0)$ . To the first order, the increase (or decrease) of sound celerity at the peaks can be expressed by:

$$\Delta c_+(t) = \frac{\beta A_+(t)}{2\rho_0 c_0}, \text{ and } \Delta c_-(t) = \frac{\beta A_-(t)}{2\rho_0 c_0} \quad (5.7)$$

Before shock formation, the signal amplitude obeys cylindrical decay rules:

$$A_+(t) = \frac{A_+(0)}{\sqrt{c_0 t}}, \text{ and } A_-(t) = \frac{A_-(0)}{\sqrt{c_0 t}} \quad (5.8)$$

With equations 5.7 and 5.8 an expression can be found for the distances from the peak to the ends of the signal:

$$d_+(0) = \int_0^{\tau_+} \frac{A_+(t) \beta}{2\rho_0 c_0} t dt, \text{ and } d_-(0) = \int_0^{\tau_-} \frac{A_-(t) \beta}{2\rho_0 c_0} t dt \quad (5.9)$$

From the above integral, equations for  $\tau_+$  and  $\tau_-$ , the shock formation times, are set:

$$\tau_+ = \sqrt[3/2]{\frac{3\rho_0 c_0^{3/2} d_+}{A_+(0) \beta}}, \text{ and } \tau_- = \sqrt[3/2]{\frac{3\rho_0 c_0^{3/2} d_-}{A_-(0) \beta}} \quad (5.10)$$

Three phases in the wave propagation can be denoted:

1. Before any shock formation:  $t < \tau_+ < \tau_-$ : no increase of signal duration.
2. After front shock formation and before back shock formation:  $\tau_+ < t < \tau_-$ : increase in signal duration is only due to positive amplitude shock.

3. After back shock formation:  $\tau_+ < \tau_- < t$ : increase in signal length is due to both shocks.

Dissipation at the shocks must be taken into account in the expression of the amplitudes. Once the shocks are formed, peak amplitudes decrease at a faster rate than simple cylindrical decay. A correction term is added to the expressions in equation 5.8:

$$\begin{aligned} A_{+,d}(t_n) &= \frac{A_+(0)}{\sqrt{c_0 t}} - \frac{A_+^2(t_{n-1}) dt\beta}{2\rho_0 c_0 (L_{ini} + d_+(t_{n-1}))} \text{ for } t > \tau_+ \\ A_{-,d}(t_n) &= \frac{A_-(0)}{\sqrt{c_0 t}} - \frac{A_-^2(t_{n-1}) dt\beta}{2\rho_0 c_0 (L_{ini} + d_-(t_{n-1}))} \text{ for } t > \tau_- \end{aligned} \quad (5.11)$$

This correction term arise from geometrical considerations. It allows to approximate dissipation effects with the help of the peak amplitudes and distances from peaks to signal ends at the previous time step. The increase of signal length can now be calculated:

$$\Delta L(t) = \begin{cases} 0 & \text{if } t < \tau_+ < \tau_- \\ \Delta c_+(t)(t - \tau_+) & \text{if } \tau_+ < t < \tau_- \\ [\Delta c_+(t) + \Delta c_-(t)] [2t - (\tau_+ + \tau_-)] & \text{if } \tau_+ < \tau_- < t \end{cases}$$

In the model above, constant sound speed is used. Spatially-varying wave celerity could be used by taking the extreme cases:  $c_0$  is replaced by  $\max(c(x, z))$  for the positive peak and  $c_0$  is replaced by  $\min(c(x, z))$  for the negative peak. This choice doesn't lead to accurate results, but the time  $t_{90}$  found can't be lower than the exact  $t_{90}$  and thus leads to efficient coupling.

#### 5.4.2. Results

The model has been used with the initial conditions and configuration presented in section 5.1. Table 5.4.2 sums up the six parameters used for the source signal and the meteorological conditions are those found in section 5.1.

The evolution of signal lengths ratio (linear/nonlinear) are calculated and shown on Figure 5.7. Both curves follow the same variations. The prediction from the model present slightly higher values (dashed line), especially when nonlinear effects are strong, at the beginning of the simulation. As nonlinear effects become weak, both curves tend to the same asymptotic value. The coupling value has been previously set to the time  $t_{90}$  where 90 % of nonlinear effects have already been taken into account. According to the numerical simulation, this time was  $t_{90} = 54$  s; with the prediction model we find  $t_{90} = 73$  s. Values are quite different due to the fact that the curves are very flat: a small difference on the y-axis leads to great variations on the x-axis. In spite of these variations on numerical values the model established reproduces the variations of the signal length with a good accuracy. Its simplicity (only 6 values describing the source

Signal property	Value
$A_+(0)$ [kPa]	49
$A_-(0)$ [kPa]	1.65
$d_+(0)$ [m]	6.21
$d_-(0)$ [m]	23.30
$L_+(0)$ [m]	23.42
$L_-(0)$ [m]	37.29

Table 5.3.: Signal properties used for the prediction model.

signal) makes it a powerful tool to estimate on which area/time range nonlinearities have substantial effects.

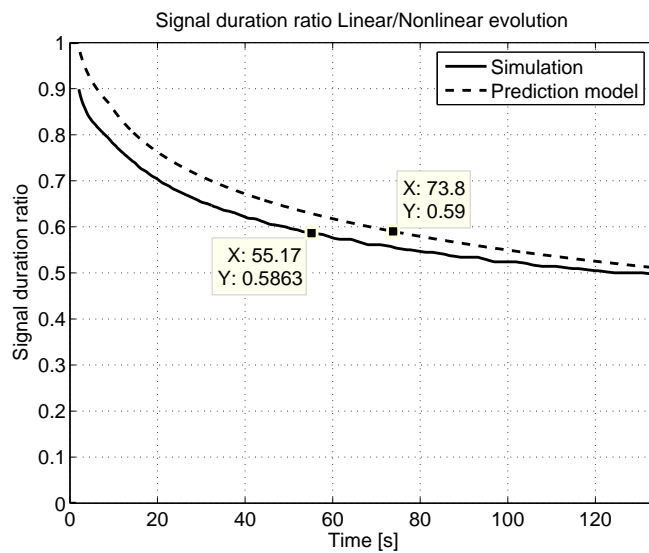


Figure 5.7.: Evolution of signal duration ratio for prediction model and simulation.



## 6. Conclusion and perspectives

### 6.1. Conclusion

The implemented nonlinear progressive wave equation has been proven to give excellent results for the problems considered. This tool allows to simulate high-amplitude sound waves in a complex environment with a good accuracy. The assumptions on which the method is based, one-way propagation and finite-length signals, lead to fast computation: even for very complex and large computations only some hours are needed to complete the simulation.

Although used algorithms are very different, the coupling between the NPE and a parabolic equation implementation turned out to give excellent results with the coupling criteria value described in section 5.3. The simple analytical model developed allows to get an estimation of the strength of nonlinearities for a specific problem. Although these simple formulas can't be used for complex configurations, it can help to know when to stop the calculations or to couple two different software.

Nonlinearities have been shown to have an important effect on high amplitude sound propagation. Signals are greatly modified: time signals characteristics as well as signals frequency content can vary a lot. This could be of importance regarding applications. Buildings in sensitive areas, where explosions can happen, could receive a special treatment compared to unexposed structures. Protection screens can also be designed in accordance to the signals characteristics.

These six months of work lead to a friendly and powerful tool. The user interfaces developed (see appendix B) and the program features will enable the CSTB to study high amplitude sound propagation problems, where nonlinearities play an important role.

### 6.2. Perspectives

The nonlinear progressive wave equation presented through this document could be improved in many ways. First non rigid grounds can be implemented. Impedance models for finite-difference time domain simulations have recently been introduced by Heutschi [31]. The polynomial representation of ground impedance explained in this article avoid the long and complex convolution previously needed to use frequency dependant impedance models.

Non flat ground could also be implemented: several methods exists: Heimann [33] developed an Eulerian finite difference time domain propagation model with terrain following coordinates: the topography is taken into account with the help of a transformation in the sound celerity expression.

The absorption layer boundary condition could also be improved: the typical thickness of this layer is about a quarter of the physical domain; the additional computational time is extremely important. Berenger [8] developed a very efficient absorbing boundary condition for electromagnetic waves: the perfectly matched layer. This absorbing boundary condition allows to absorb outgoing wave with a single layer. This method has recently been adapted to acoustic finite difference simulations (see Hu [21]) and could be implemented on the nonlinear progressive wave equation.

During this master's thesis only one numerical model has been coupled to the NPE: ATMOS, a software that solves for linear propagation. The CSTB owns very accurate tools to study sound propagation. Boundary element methods and the nonlinear progressive wave equation could be combined to allow modeling the propagation over complex surfaces.

# Bibliography

- [1] Aanonsen. Distortion and harmonic generation in the nearfield of a finite amplitude sound beam. *Journal of the Acoustical Society of America*, 75(2), 1984.
- [2] F. Aballéa. *Propagation acoustique en milieu extérieur: application de l'équation parabolique rapide au couplage d'effets météorologiques et de topographies complexes*. PhD thesis, Université du Maine, Le Mans, France, 2004.
- [3] K. Attenborough. Acoustical impedance models for outdoor ground surfaces. *Journal of Sound And Vibrations*, 99(4), 1985.
- [4] K. Attenborough. Ground parameter information for propagation modelling. *Journal of the Acoustical Society of America*, 92(1), 1992.
- [5] K. Attenborough. Benchmark cases for outdoor sound propagation models. *Journal of the Acoustical Society of America*, 97(1), 1995.
- [6] T. Van Renterghem B. de Greve and D. Botteldooren. Long range fdtd over undulating terrain. Technical report, 2005.
- [7] P. Caine B.E. McDonald and M. West. A tutorial on the nonlinear progressive wave equation (npe) - part 1. *Applied Acoustics*, 43(159-167), 1994.
- [8] J. P. Berenger. A perfectly matched layer for the absorption of electromagnetic waves. *Journal of Computational Physics*, 114, 1994.
- [9] C. Bogey and C. Bailly. Three-dimensional non-reflective boundary conditions for acoustic simulations: far field formulation and validation cases. *Acta Acustica united with Acustica*, 88, 2002.
- [10] J. P. Boris and D. L. Book. Shasta - a fluid transport algorithm that works. *Journal of Computational Physics*, 135, 1997.
- [11] P. Caine and M. West. A tutorial on the nonlinear progressive wave equation (npe) - part 2. derivation of the three dimensional cartesian version without use of perturbation expansions. *Applied Acoustics*, 45(155-165), 1995.
- [12] B. D. Cook. New procedure for computing finite amplitude distortion. *Journal of the Acoustical Society of America*, 34(7), 1962.

- [13] A. Piacsek D. B. Clarke and J. W. White. Predictions of acoustic signals from explosions above and below the ocean surface: source region calculations. Technical report, 1996.
- [14] M. Möller D. Kuzmin and S. Turek. Implicit flux-corrected transport algorithm for finite element simulation of the compressible euler equations. Technical report, 2002.
- [15] F. Van Der Eerden and E. Védy. Propagation of shock waves from source to receiver. *Noise Control Engineering Journal*, 53(3), 2005.
- [16] T.F.W. Embleton. Tutorial on sound propagation outdoors. *Journal of the Acoustical Society of America*, 100(1), 1996.
- [17] B. O. Enflo and C. M. Hedberg. *Theory of Nonlinear Acoustics in Fluids*. Kluwer Academic publishers, 2002.
- [18] M. A. Etaati. An absorbing layer for non-linear wave equations: First order formulation. Master's thesis, 1990.
- [19] J. van 't Hof F. Van Der Eerden, F. Van Den Berg and E. Van Arkel. A blast absorber test: measurement and model results. Tampere, Finland, June 2006. Euronoise 2006.
- [20] M. F. Hamilton and D. T. Blackstock. *Nonlinear Acoustics*. Academic Press, 1998.
- [21] F. Hu. A perfectly matched layer absorbing condition for linearized euler equations with a non-uniform mean ow. *Journal of Computataional Physics*, 208, 2005.
- [22] M. Y. Hussaini I.M. Navon, B. Neta. A perfectly matched layer formulation for the nonlinear shallow water equations models: The split equation approach. Technical report, 2001.
- [23] U. Ingård. A review of the influence of meteorological effects conditions on sound propagation. *Journal of the Acoustical Society of America*, 25(3), 1953.
- [24] Y. Inoue and T. Yano. Propagation of strongly nonlinear plane waves. *Journal of the Acoustical Society of America*, 94(3), 1993.
- [25] E. S. Oran J. P. Boris, A. M. Landsberg and J. H. Gardner. *LCPFCT - Flux corrected transport algorithm for solving generalized continuity equations*, 1993.
- [26] G. P. James and J. H. Ginsberg. Nonlinear progressive wave equation model for transient and steady state sound beams. *Journal of the Acoustical Society of America*, 91(1), 1992.

- [27] B.E. McDonald J.J. Ambrosiano, D.R. Plante and W.A. Kuperman. Nonlinear propagation in an ocean acoustic waveguide. *Journal of the Acoustical Society of America*, 87(4), 1990.
- [28] E. Védy K. Attenborough, P. Schomer and F. Van Der Eerden. Overview of the theoretical development and experimental validation of blast sound-absorbing surfaces. *Noise Control Engineering Journal*, 53(3), 2005.
- [29] G. D'Spain B.E. McDonald K. Castor, P. Gerstoft and W.A. Kuperman. Nonlinear effects in long range propagation. Technical report, 2002.
- [30] P. Roux B.E. McDonald K. Castor, P. Gerstoft and W.A. Kuperman. Long-range propagation of finite-amplitude acoustic waves in an ocean waveguide. *Journal of the Acoustical Society of America*, 116(4), 2004.
- [31] M. Horvath K. Heutschi and J. Hofmann. Simulation of ground impedance in finite difference time domain calculations of outdoor sound propagation. *Acta Acustica united with Acoustica*, 91, 2005.
- [32] M. Kamegai and J. W. White. A study of near-surface and underwater explosions by computer simulations. Technical report, 1994.
- [33] R. Karle and D. Heimann. A linearized eulerian nite difference time domain sound propagation model with terrain following coordinates. *Journal of the Acoustical Society of America*, 119(6), 2006.
- [34] G.F. Kinney and J. Graham. *Explosive shocks in air*. Springer Verlag, 1988.
- [35] Y. S. Lee. *Numerical solution of the KZK equation for pulsed finite amplitude sound beams in thermoviscous fluids*. PhD thesis, 1993.
- [36] Y. S. Lee and M. F. Hamilton. Time-domain modeling of pulsed finite-amplitude sound beams. *Journal of the Acoustical Society of America*, 97(2), 1995.
- [37] B.E. McDonald. Weak shock interaction with a free-slip interface at low grazing angles. *Journal of the Acoustical Society of America*, 91(2), 1992.
- [38] B.E. McDonald. High-angle formulation for the nonlinear progressive wave equation model. *Wave Motion*, 31(165-171), 2000.
- [39] B.E. McDonald and W. A. Kuperman. Time domain formulation for pulse propagation including nonlinear behaviour at a caustic. *Journal of the Acoustical Society of America*, 81(5), 1987.

- [40] A.A. Atchley M.S.Wochner and V.W. Sparrow. Numerical simulation of finite amplitude wave propagation in air using a realistic atmospheric absorption model. *Journal of the Acoustical Society of America*, 118(5), 2005.
- [41] R.E. Munn. *Descriptive micrometeorology*. Academic, New York, 1966.
- [42] D. K. Wilson D. H. Marlin S. L. Collier N. P. Symons, D. F. Aldridge and V. E. Ostashev. Finite difference simulation of atmospheric acoustic sound through a complex meteorological background over a topographically complex surface. Tampere, Finland, June 2006. Euronoise 2006.
- [43] C. Peng and M. N. Toksoz. An optimal absorbing boundary condition for finite difference modeling of acoustic and elastic wave propagation. *Journal of the Acoustical Society of America*, 95(2), 1994.
- [44] A.D. Pierce. *Acoustics: an introduction to its physic principles and applications*. *Acoustical Society of America, New york*, 1989.
- [45] J.E. Piercy and T.F.W. Embleton. Review of noise propagation in the atmosphere. *Journal of the Acoustical Society of America*, 61(6), 1977.
- [46] H.E. Bass R. Raspet D.T. Blackstock R.O. Cleveland, J.P. Chambers and M.F. Hamilton. Comparison of computer codes for the propagation of sonic boom waveforms through isothermal atmospheres. *Journal of the Acoustical Society of America*, 100(5), 1996.
- [47] M. Hamilton R.O. Cleveland and D.T. Blackstock. Time-domain modeling of finite-amplitude sound in relaxing fluids. *Journal of the Acoustical Society of America*, 99(6), 1996.
- [48] P.H. Rogers. Weak shock solution for underwater explosive shock waves. *Journal of the Acoustical Society of America*, 62(6), 1977.
- [49] E.M. Salomons. *Computational atmospheric acoustics*. Kluwer Academic, 2001.
- [50] N. Sepasian. An absorbing layer for non-linear wave equations: Second order formulation. Master's thesis, 2006.
- [51] B. Sjögreen. Lecture notes on shock capturing difference methods. Technical report, 1990.
- [52] V.W. Sparrow and R. Raspet. A numerical method for general finite amplitude wave propagation in two dimensions and its application to spark pulses. *Journal of the Acoustical Society of America*, 90(5), 1991.

- [53] L.C. Sutherland and H. E. Bass. Atmospheric absorption in the atmosphere up to 160 km. *Journal of the Acoustical Society of America*, 115(3), 2004.
- [54] G.P.J. Too and S. T. Lee. Thermoviscous effects on transient and steady-state sound beams using nonlinear progressive wave equation models. *Journal of the Acoustical Society of America*, 97(2), 1995.
- [55] G. Toth and D. Odstrcil. Comparison of some flux corrected transport and total variation diminishing numerical schemes for hydrodynamic and magnetohydrodynamic problems. *Journal of Computational Physics*, 128, 1996.
- [56] L. Liu D. F. Aldridge N. P. Simons V. E. Ostashev, K. Wilson and D. Marlin. Equations for finite difference, time domain simulation of sound propagation in moving inhomogeneous media and numerical implementation. *Journal of the Acoustical Society of America*, 117(2), 2005.
- [57] E. Védý. Numerical simulation of strong shocks. *Noise Control Engineering Journal*, 50(6), 2002.
- [58] E. Védý. Simulation of flows in porous media with a flux corrected transport method. *Noise Control Engineering Journal*, 50(6), 2002.
- [59] E. Védý and F. Van Der Eerden. Prediction of shock waves over a sound absorbing area. *Noise Control Engineering Journal*, 53(3), 2005.
- [60] M. Wochner. *Numerical simulation of multi-dimensional acoustic propagation in air including the effects of molecular relaxation*. PhD thesis, 2006.



# A. Crank-Nicolson scheme and Thomas algorithm

## Crank-Nicolson scheme

The Crank-Nicolson method is a finite difference scheme used to numerically solve differential equations such as the heat equation. The method was developed by John Crank and Phyllis Nicolson in the mid twentieth century. The scheme is second order in time, and stable for all  $\delta t$ . It involves taking the space derivatives half way between the beginning and the end of the time space, *i.e.*:

$$\frac{\partial u}{\partial x} \equiv \frac{1}{2} \left[ \frac{u_{i+1,j}^{n+1} - 2u_{i,j}^{n+1} + u_{i-1,j}^{n+1}}{2\delta x} + \frac{u_{i+1,j}^n - 2u_{i,j}^n + u_{i-1,j}^n}{2\delta x} \right]$$

$$\frac{\partial^2 u}{\partial x^2} \equiv \frac{1}{2} \left[ \frac{u_{i+1,j}^{n+1} - 2u_{i,j}^{n+1} + u_{i-1,j}^{n+1}}{\delta x^2} + \frac{u_{i+1,j}^n - 2u_{i,j}^n + u_{i-1,j}^n}{\delta x^2} \right]$$

It is hence an average between fully explicit and fully implicit models of PDE's. This is where the second order convergence comes from. This leads to solve a tridiagonal linear equations system that can fastly be solved with a Thomas algorithm.

## Thomas algorithm

Semi-implicit schemes require a linear system of equations to be solved where the matrix is tridiagonal. The Thomas algorithm is an efficient method to solve the system  $Bu = d$  where  $B$  is tridiagonal and of size  $N \times N$ .

$$B = \begin{pmatrix} \alpha_1 & \beta_1 & & & \\ \gamma_1 & \alpha_2 & \beta_2 & & \\ & \ddots & \ddots & \ddots & \\ & & \gamma_{N-2} & \alpha_{N-1} & \beta_{N-1} \\ & & & \gamma_{N-1} & \alpha_N \end{pmatrix} \quad (\text{A.1})$$

The Thomas algorithm is decomposed in three steps:

1. A LR decomposition.

2. A forward substitution.
3. A backward substitution.

### First step: LR decomposition

The matrix  $B$  can be decomposed in a lower bidiagonal matrix and an upper bidiagonal matrix:

$$L = \begin{pmatrix} 1 & & & & \\ l_1 & 1 & & & \\ & \ddots & \ddots & & \\ & & & l_{N-1} & 1 \end{pmatrix}$$

$$R = \begin{pmatrix} m_1 & r_1 & & & \\ & \ddots & \ddots & & \\ & & & m_{N-1} & r_{N-1} \\ & & & & m_N \end{pmatrix}$$

One can note that  $r_i = \beta_i$  for all  $i$ ; the coefficients  $m_i$  and  $l_i$  can be obtained as follow:

$$m_1 := \alpha_1$$

For  $i = 1, 2, \dots, N$  do:

$$l_i := \gamma_i / m_i$$

$$m_{i+1} := \alpha_{i+1} - l_i \beta_i$$

### Second step: forward substitution

The system  $Ly = d$  is solved; we get:

$$y_1 := d_1$$

For  $i = 2, \dots, N$  do:

$$y_i := d_i - l_{i-1} y_{i-1}$$

### Third step: backward substitution

The system  $Ru = y$  is solved; we get:

$$u_N := y_N / m_N$$

For  $i = N - 1, N - 2, \dots, 1$  do:

$$u_i := (y_i - \beta_i u_{i+1}) / m_i$$

## **B. User interface to the NPE propagation code**

Four user interfaces have been created to interact with the NPE code. Developed with Matlab, it allows to use the simulation program in an easy way.

The first interface (see Figure B.1) is used to enter parameters such as window length and spatial steps, medium properties or sound speed profile. This interface writes a file on the disk that will be read by the program.

Another interface allows to easily create input signals (see Figure B.2). Several kind of signals can be designed either with the help of analytical expression (Matlab syntax) or by loading Matlab array files. A file containing signal data is written and then read during program execution.

The third interface (see Figure B.3) is used to visualize results. It can be used to plot transmission loss or excess attenuation maps, time signals at the receivers or snapshots at recorded time steps.

The last interface can be used to facilitate the use and configuration of ATMOS in case of a coupling between the NPE code and ATMOS (see Figure B.4). It allows to transform time signals into frequency domain starter that can be directly used in ATMOS.

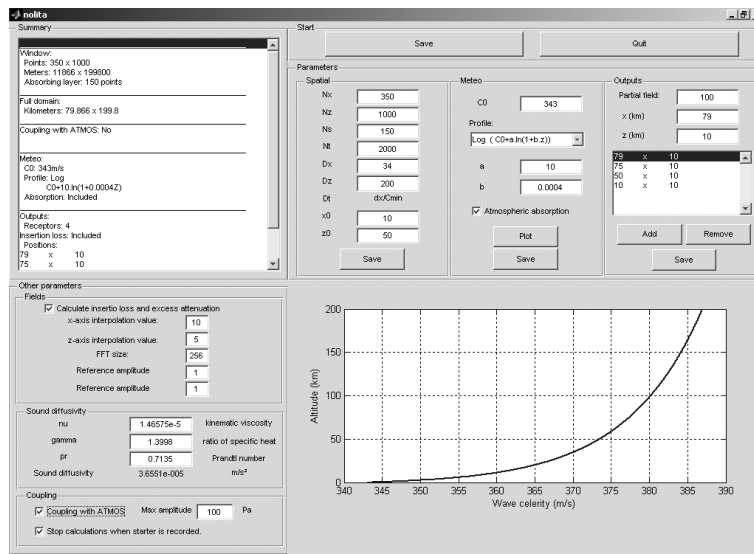


Figure B.1.: Parameters interface.

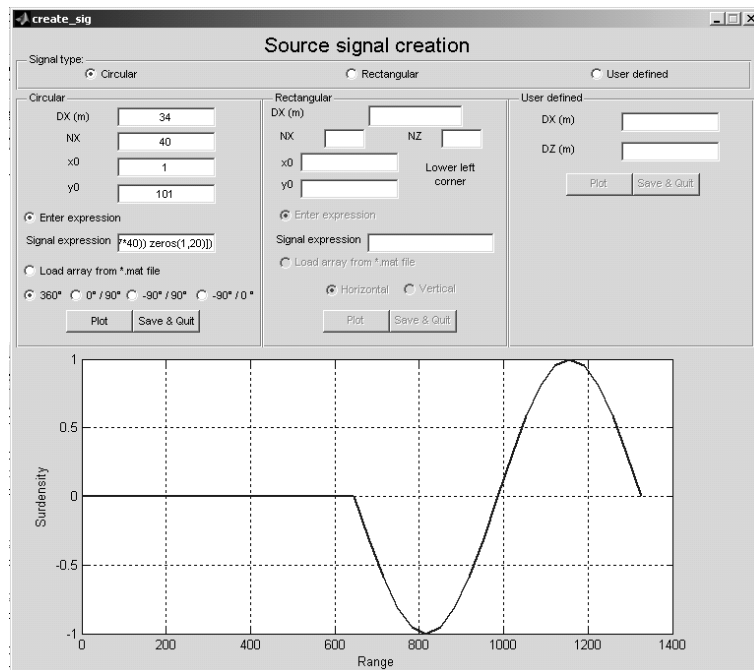


Figure B.2.: Source signal creation interface.

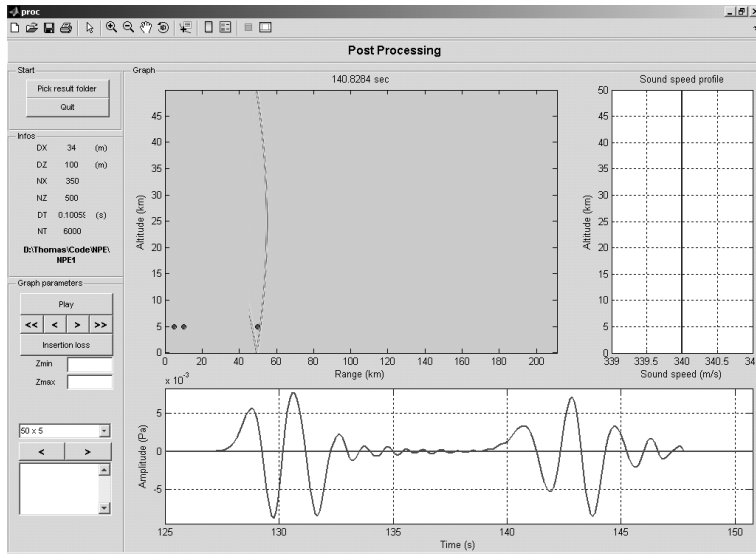


Figure B.3.: Post processing interface.

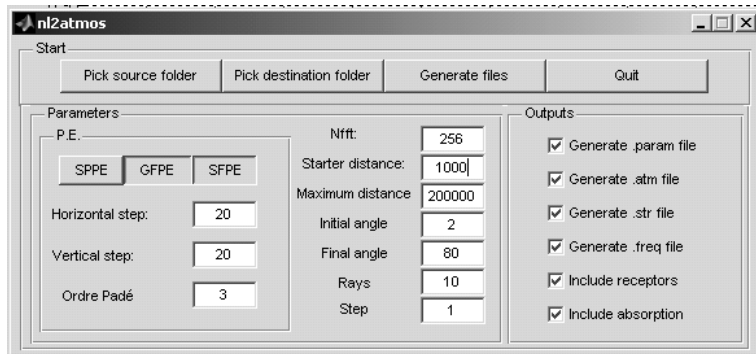


Figure B.4.: Coupling interface.